ATMOSPHERIC SCIENCE

# Chemistry and human exposure implications of secondary organic aerosol production from indoor terpene ozonolysis

**Colleen Marciel F. Rosales[1]†, Jinglin Jiang[2,3], Ahmad Lahib[1,4], Brandon P. Bottorff[5], Emily K. Reidy[5], Vinay Kumar[1], Antonios Tasoglou[6], Heinz Huber[6,7], Sebastien Dusanter[4], Alexandre Tomas[4], Brandon E. Boor[2,3]*, Philip S. Stevens[1,5]***



**Surface cleaning using commercial disinfectants, which has recently increased during the coronavirus disease 2019 pandemic, can generate secondary indoor pollutants both in gas and aerosol phases. It can also affect indoor air quality and health, especially for workers repeatedly exposed to disinfectants. Here, we cleaned the floor of a mechanically ventilated office room using a commercial cleaner while concurrently measuring gas-phase precursors, oxidants, radicals, secondary oxidation products, and aerosols in real-time; these were detected within minutes after cleaner application. During cleaning, indoor monoterpene concentrations exceeded outdoor concentrations by two orders of magnitude, increasing the rate of ozonolysis under low (<10 ppb) ozone levels. High number concentrations of freshly nucleated sub–10-nm particles (≥$10^5$ $cm^{-3}$) resulted in respiratory tract deposited dose rates comparable to or exceeding that of inhalation of vehicle-associated aerosols.**

## INTRODUCTION

Atmospheric particle pollution is understood to result from either primary (direct) emissions such as from combustion (*1*, *2*) or from secondary chemical formation through the oxidation of volatile organic compounds (VOCs) (*3*–*5*). The latter requires an understanding of the chemical mechanisms of numerous gas-phase organic and inorganic reactions. Previous indoor studies have shown that, in addition to human-induced resuspension of dust (*6*), both primary emissions and secondary chemical formation can also be important sources of indoor particles (*7*–*16*). In contrast to the outdoor environment, indoor new particle formation (NPF) is inherently influenced by building-related factors, such as (i) ventilation conditions; (ii) air cleaning and filtration; (iii) high surface area–to–volume ratios; (iv) the abundance of surfaces that serve as sinks, sources, or media for heterogeneous chemistry for particles and reactive gases; and (v) nonphotolytic radical sources (*7*–*10*, *17*–*19*). The indoor environment is highly dynamic and easily perturbed by human activities and occupancy patterns. Indoor NPF events can occur at time scales shorter than that of the outdoors (e.g., seconds to minutes rather than hours) and are thus less likely to achieve steady-state concentrations for extended periods.

One perturbation that humans introduce to the indoor environment is the use of household cleaning and disinfection products, some of which have "natural" scents, such as citrus or pine. These products are important sources of VOCs indoors. Limonene, a monoterpene, is a commonly used chemical in household cleaning products because of its citrus scent, high capacity as a solvent to hold dirt, high versatility and applicability to different surfaces, and pesticidal properties (*20*). Consequently, it has been found in indoor air at concentrations ranging from 20 to 50 μg $m^{-3}$ [~4 to 9 parts per billion (ppb)] in residential buildings (*21*) and peaking at over 70 μg $m^{-3}$ (~13 ppb) during cleaning episodes (*7*). As primary emissions, cleaning-associated VOCs may cause sensory irritation, headaches, damage to organs, or cancer (*22*).

VOCs emitted by household cleaning products may be oxidized by indoor oxidants, such as ozone ($O_3$), or radicals, such as hydroxyl (OH), nitrate ($NO_3$), or chlorine (Cl) (*17*–*19*, *23*), although indoor VOC oxidation is dominated by $O_3$ and OH (*18*, *19*). These reactions can lead to the formation of peroxides, alcohols, carbonyls, carboxylic acids, and other low-volatility, highly oxidized organic compounds (*5*, *18*) that can nucleate, accumulate, and grow a class of particles called secondary organic aerosol (SOA). Indoors, $O_3$ mostly reacts with terpenes (e.g., limonene, one of the most reactive terpenes with $O_3$), terpenoids, squalene, and unsaturated fatty acids found in skin oil and cooking oils (*24*, *25*). Meanwhile, OH reacts with a variety of VOCs, including terpenes (limonene and others), alcohols, aldehydes, and aromatics (*19*). While indoor VOCs may be present because of building material emissions during noncleaning periods, the use of household cleaners may further increase VOC concentrations (*11*) to levels comparable to, or greater than, environments where SOA formation induced either by ozonolysis or oxidation by OH radicals has been observed (*3*).

While it is well established that the ozonolysis of monoterpenes leads to the production of atmospheric SOA (*3*), ozonolysis-initiated indoor SOA formation is not often seen as a dominant indoor particle source, as the indoor environment is typically insulated from outdoor $O_3$ because of $O_3$ losses to the surfaces of ventilation systems, building envelope components, interior walls and furnishings,

[1]O'Neill School of Public and Environmental Affairs, Indiana University, Bloomington, IN 47405, USA. [2]Lyles School of Civil Engineering, Purdue University, West Lafayette, IN 47907, USA. [3]Ray W. Herrick Laboratories, Center for High Performance Buildings, Purdue University, West Lafayette, IN 47907, USA. [4]IMT Lille Douai, Institut Mines-Télécom, Université de Lille, Center for Energy and Environment, 59000 Lille, France. [5]Department of Chemistry, Indiana University, Bloomington, IN 47405, USA. [6]RJ Lee Group Inc., Monroeville, PA 15146, USA. [7]Edelweiss Technology Solutions LLC, Novelty, OH 44072, USA.
*Corresponding author. Email: bboor@purdue.edu (B.E.B.); pstevens@indiana.edu (P.S.S.)
†Present address: Air Quality Research Center, University of California, Davis, One Shields Ave., Davis, CA 95616, USA.

human skin, and clothing (*26*). Indoor SOA formation and the associated mass loading of secondary particles apparently resulting from the oxidation of limonene by $O_3$ have been observed in reaction chambers emulating indoor conditions (*8*, *9*, *11*, *12*), in a real room with $O_3$ from outdoor air reacting with either pure limonene (*16*, *17*) or a commercial cleaning product (*7*, *13*, *16*) evaporated into the room, in a real room where $O_3$ was generated by an indoor air purifier during a cleaning episode (*7*), from peeling an orange in an enclosed room and in a museum gallery (*14*, *27*), and with limonene exposure to other household cleaning products containing HOCl and $Cl_2$ (e.g., bleach) (*23*). A few monoterpene oxidation reactions that are suspected to lead to SOA formation indoors have been parameterized on the basis of building air exchange rates (AERs) to improve the prediction of indoor SOA mass concentrations (*10*). In addition, previous modeling studies coupled with chamber (*4*) and flow reactor (*3*, *5*) studies have elucidated gas-phase oxidation products from limonene ozonolysis.

However, real-time, simultaneous observations under realistic indoor conditions that show SOA formation and growth from these secondary oxidation products have been sparse (*7*, *11*, *13*). In addition, distinguishing indoor NPF from primary particle emissions and prediction of NPF events remain challenging because of the lack of information on gas-particle partitioning (*18*) and measurements of gas-phase intermediates, such as low-volatility organics and radicals. Moreover, indoor measurements of radical intermediates have not been directly associated with indoor SOA formation. While there have been a few measurements of indoor radical concentrations, including OH and $HO_2$ concentrations during cleaning episodes (*28*) or in unoccupied classrooms (*29*, *30*), we present here the first measurements that track the formation of indoor OH, $HO_2$, and $RO_2$ radicals and secondary oxidation products from the ozonolysis of monoterpenes and monoterpenoids and the subsequent rapid formation of nanoparticles during an indoor mopping event.

A commercial monoterpene-based household cleaner was used to mop and wipe surfaces inside an enclosed, mechanically ventilated test room in a research building in a forested area for 12 to 14 min to emulate real cleaning conditions. OH and peroxy ($HO_2$ and $RO_2$) radicals were measured together with VOCs, including monoterpenes, monoterpenoids, gas-phase secondary oxidation products, $O_3$, and $NO_x$ (NO and $NO_2$). Particle number size distributions were measured using a suite of aerosol instrumentation that cover particle diameters from 1.2 to 10,000 nm, encompassing the nanocluster (1.2 to 3 nm), nucleation (3 to 10 nm), Aitken (10 to 100 nm), accumulation (100 to 2500 nm), and coarse (2500 to 10,000 nm) modes. The influence of photolytic oxidant sources was determined by performing the cleaning events under both direct and indirect sunlight conditions. Measured radicals and gas-phase products were then compared to predicted concentrations using an established modeling framework. SOA mass concentrations were predicted using a single-zone mass balance approach to compare to concentrations measured during the mopping episodes. Furthermore, to assess human inhalation exposure and dose for the newly formed particles, size-resolved respiratory tract deposited dose rates (RTDDRs) were analyzed for the mopping events and suggest that indoor SOA production due to monoterpene ozonolysis during mopping may lead to dose rates greater than, or comparable to, what one would receive outdoors in urban environments.

## RESULTS

### Indoor observations of the rapid formation of peroxy radicals and NPF following episodic monoterpene emissions during mopping events

A simplified chemical reaction scheme for the oxidation of VOCs is shown in Fig. 1. Direct (primary) emissions of VOCs were observed using a proton transfer reaction time-of-flight mass spectrometer (PTR-ToF-MS) during two mopping periods and are shown in Figs. 2A and 3A. Monoterpene concentrations are expressed as a sum of the signals detected at mass/charge ratio (*m*/*z*) 81 and *m*/*z* 137, which represent a known fragment $(C_6H_9)^+$ and the protonated mass $(C_{10}H_{16})H^+$, respectively, and can be from a variety of monoterpenes

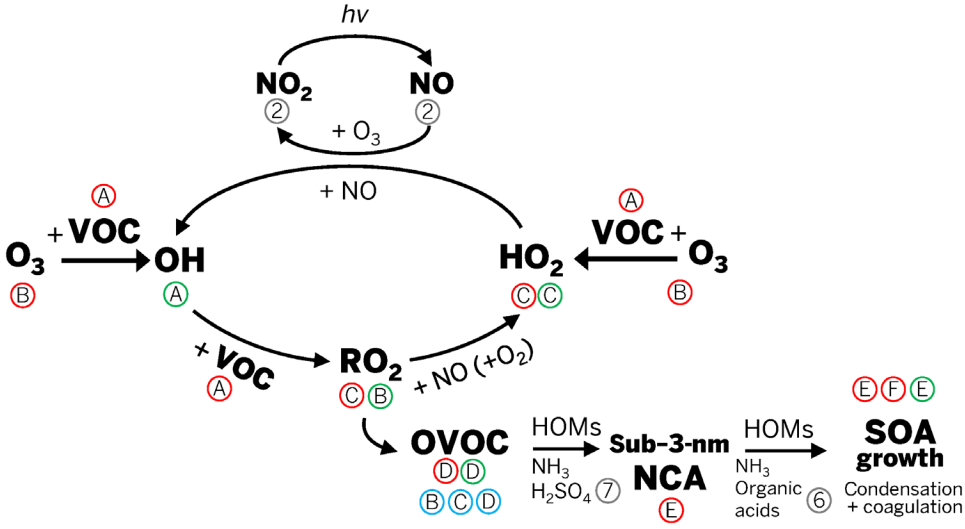


**Fig. 1. Simplified scheme for VOC ozonolysis and radical cycling leading to indoor SOA formation.** Letters in red circles correspond to panel labels in Fig. 2, letters in blue circles correspond to panel labels in Fig. 3, letters in green circles correspond to panel labels in Fig. 4, and numbers in gray circles correspond to figure numbers in the Supplementary Materials. HOMs, highly oxygenated organic molecules; NCA, nanocluster aerosol; OVOC, oxygenated VOC; *hv*, light.

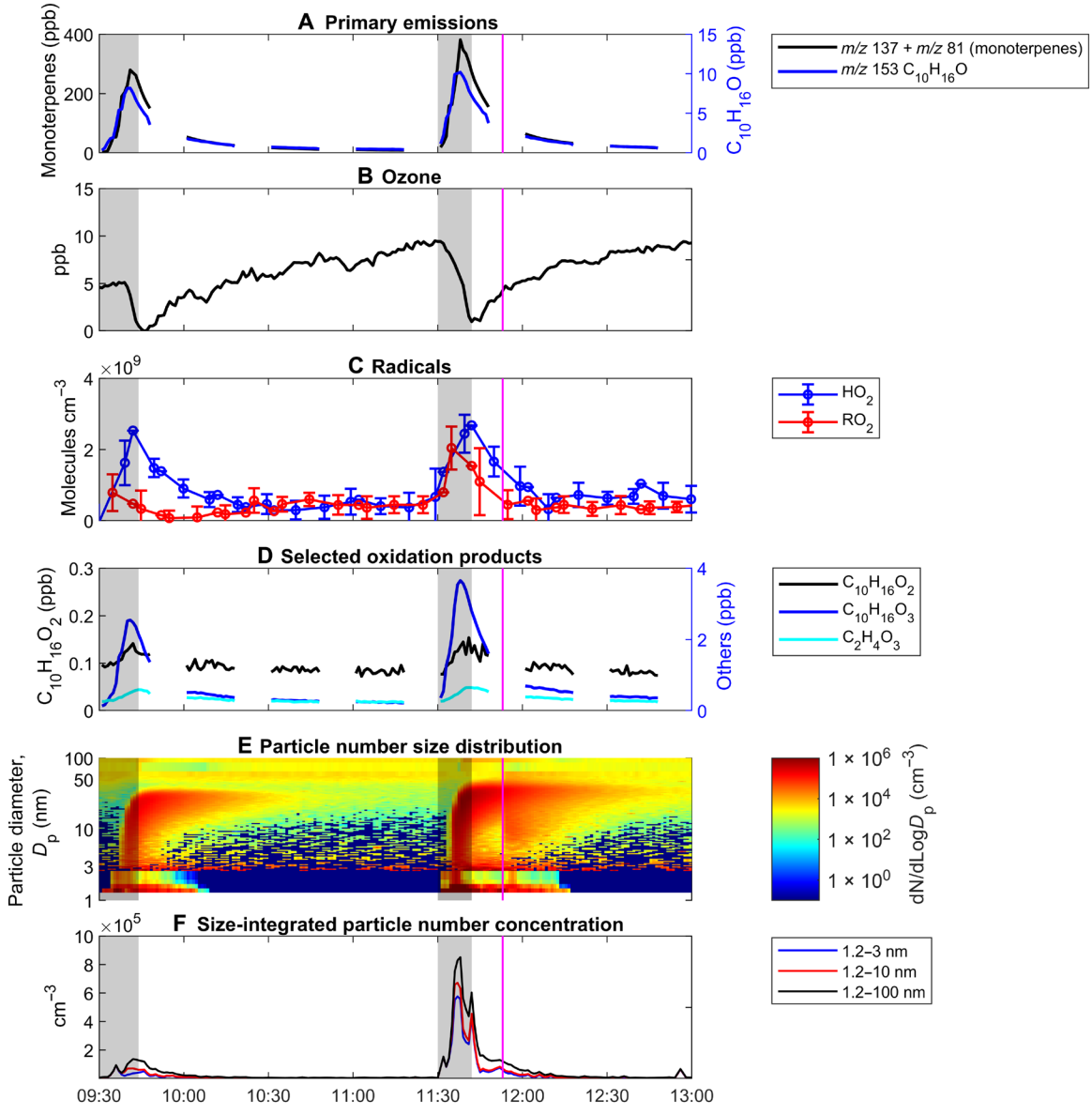


**Fig. 2. Measured chemical species during the cleaning experiments.** (**A**) Primary VOC emissions, (**B**) ozone, (**C**) $HO_2$ and $RO_2$ radicals, (**D**) selected oxidation products, (**E**) particle number size distribution, and (**F**) size-integrated particle number concentrations. Gray shading corresponds to active periods of mopping and wiping during the cleaning events. The magenta line corresponds to a $CO_2$ injection, which was done to estimate the AER of the room. The particle diameter from 1.2 to 2.5 nm is the activation diameter measured by the nano Condensation Nucleus Counter (nCNC), and the particle diameter from 2.5 to 100 nm is the electrical mobility diameter measured by the Scanning Mobility Particle Sizer (SMPS) and NanoScan SMPS.

(α- and β-pinene, limonene, camphene, myrcene, and 3-carene, among others) (*31*). Analysis by gas chromatography–electron ionization mass spectrometry (GC-MS) revealed that the liquid cleaning solution is composed of a mixture of various monoterpenes, including limonene, α-pinene, β-pinene, and camphene (table S1). $C_{10}H_{16}O$, possibly citral, is shown as *m/z* 153 in Fig. 2A. Citral, an aldehyde with a citrus odor, has been previously found as a component of other commercial cleaning products (*28*). $C_{10}H_{16}O$, along with $C_{10}H_{18}O$, can also be C10 alcohols, like α-terpineol, isoborneol, and myrcenol (isomers with molecular formula $C_{10}H_{18}O$) because C10 alcohols were also listed as ingredients in the commercial product and were detected in the GC-MS analysis. Mixing ratios of these C10 compounds are shown in Fig. 3A and fig. S6A.

During the first and second mopping periods, monoterpene mixing ratios peaked at 280 and 380 ppb, respectively (Fig. 2A); this is 140 to 190 times more than the peak outdoor monoterpene mixing ratios observed outside the research building for this day (~2 ppb). While indoor mixing ratios depend on a variety of factors, including the AER, cleaning solution concentrations, and cleaning surface area, the limonene mixing ratios observed in this study were approximately 1.3 to 2.2 times more than a lemon-scented furniture polish (wax) application to a coffee table inside a 25-m$^3$ chamber (*15*), about 1.8 to 2.4 times more than the peak limonene concentration from a household product used in a 50-m$^3$ chamber (*11*), approximately 20 times more than the peak indoor mixing ratios previously observed in an Australian classroom (~17 ppb) (*13*),

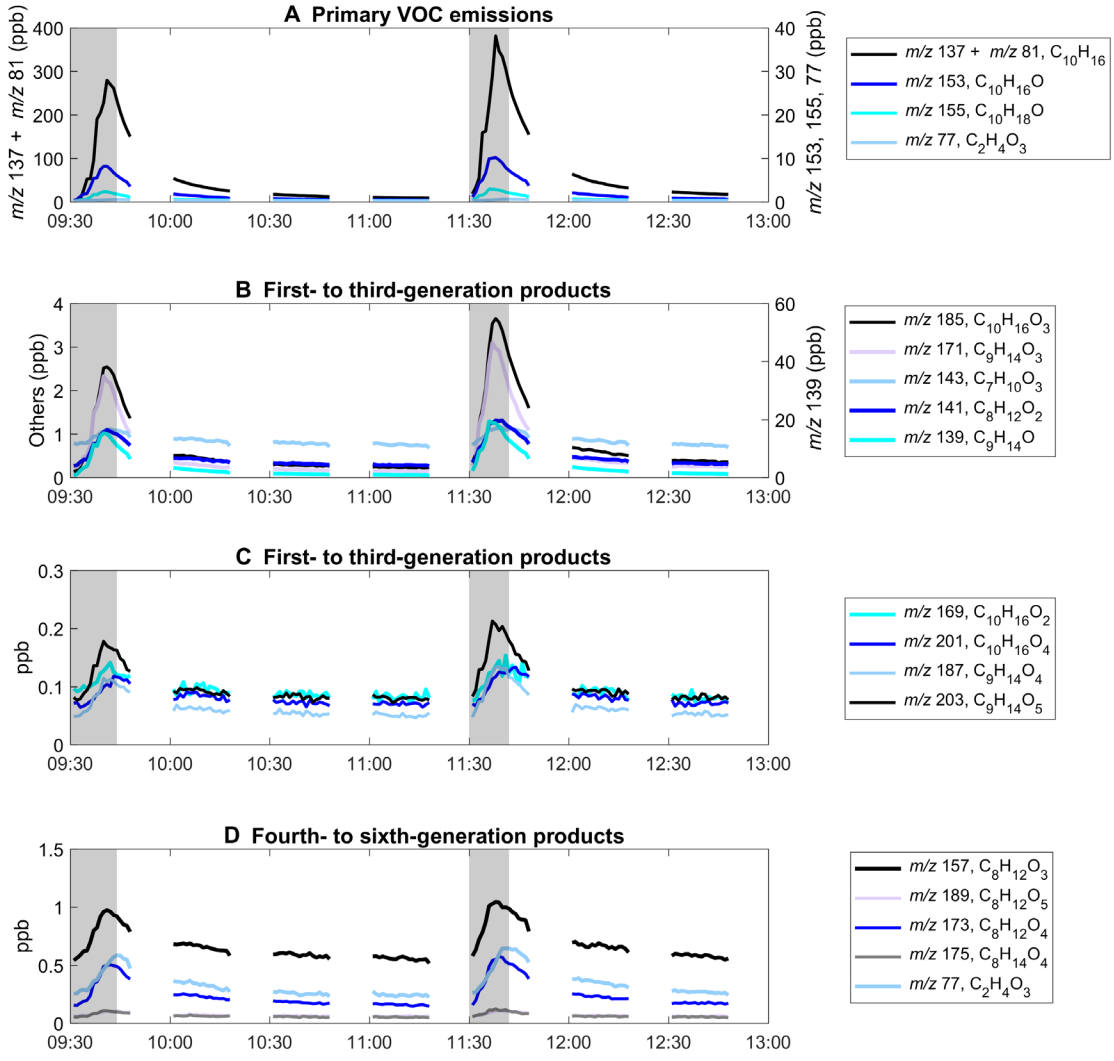


**Fig. 3. Gas-phase secondary oxidation products observed via PTR-ToF-MS measurements.** Gray shading corresponds to active periods of mopping and wiping during the cleaning events. Primary monoterpene and monoterpenoid emissions (**A**), most likely composed of limonene, α-pinene, β-pinene, and camphene (table S1), which cannot be differentiated using PTR-ToF-MS. Other gas-phase species in (**B**) to (**D**) were observed to have a slight delay in the appearance of their peaks, with respect to the mopping period and monoterpene peak, which is indicative of being a product of secondary chemical processes. Possible structures of the oxidation products are shown in table S2. Chemical pathways leading to secondary oxidation products in (B) to (D) are shown in figs. S3 and S4.

3.7 to 5 times more than monoterpene emissions from botanical disinfectants sprayed onto a glass kitchen countertop (*32*), and about 56 to 76 times more than the peak mixing ratios observed during the HOMEChem field campaign (~5 ppb) (*33*), where similar mopping experiments using a monoterpene-based cleaner were done. The volume of the HOMEChem test house was larger (250 $m^3$) as compared to the room used in this study (~50 $m^3$); thus, the emissions from the mopping events dispersed into a larger volume, resulting in lower concentrations during the mopping episode. Concomitantly, indoor $O_3$ decreased to less than 1 ppb during the mopping event, from initial background concentrations of about 5 and 10 ppb for the first and second mopping events, respectively (Fig. 2B). After the steep decline, indoor $O_3$ concentrations slowly increased as a result of outdoor air introduction via mechanical ventilation. This contrasts with chamber SOA studies where $O_3$ is usually in excess; these short bursts or "pulses" introduced by the mopping events are similar to a rapid injection of VOCs in chamber studies but within a more realistic indoor scenario, i.e., a real room with mechanical ventilation in an occupied building.

Other compounds known in the ambient environment that can be oxidized leading to SOA formation, such as isoprene and sesquiterpenes, were also detected. Background isoprene (*m/z* 69) and a lower limit to sesquiterpene (*m/z* 205, parent ion only) mixing ratios in the room were about 7 and 0.2 ppb, respectively. During the first mopping event, they increased to 13 and 0.8 ppb, respectively; for the second mopping event, they increased to 19 and 1 ppb, respectively. Isoprene likely originated from the exhaled breath of the person mopping (*34*) or from the ambient forest environment, where isoprene was previously observed to be on the order of 1 to 4 ppb (*35*). On the other hand, the sesquiterpenes were likely emitted directly from the cleaning product, which contained pine oil (*36*). While these compounds are also known to be SOA precursors, indoor oxidants ($O_3$ and OH) are most likely to react with limonene and

other monoterpenes and form peroxy radicals and particles because of their much higher abundance relative to isoprene and sesquiterpenes.

Figure 2C shows the subsequent increase in the $HO_2$ and $RO_2$ radical concentrations after the mopping event, peaking near $2 \times 10^9$ to $3 \times 10^9$ molecules $cm^{-3}$, higher than the maximum total $HO_2 + RO_2$ concentration of approximately $1 \times 10^9$ molecules $cm^{-3}$ previously measured in the outdoor forested area of the research building where the test room was located (*37*). In addition, the observed $HO_2$ concentration was about two orders of magnitude higher than that measured in an unoccupied classroom in Marseille, France, where the $HO_2$ concentration was reported to be $0.6 \times 10^7$ to $3.7 \times 10^7$ molecules $cm^{-3}$ (*29*). While this is not the first time that these radicals have been measured indoors, it is the first time that concentrations of $HO_2$ and $RO_2$ have been measured as a result of $O_3$/terpene chemistry using a commercial cleaner in an indoor setting. The increase in radical concentrations did not correlate with changes in the amount of direct sunlight to the room, as represented by the measurements of the $NO_2$ photolysis frequency, $J_{NO2}$ (fig. S2). Rather, $HO_2$ and $RO_2$ concentrations during the mopping events increased as the monoterpene concentrations increased and the $O_3$ concentration decreased, suggesting that the radical concentrations were not derived from photolysis but produced solely from monoterpene ozonolysis. While the measured concentration of $HO_2$ radicals was similar during the two mopping events, the concentration of $RO_2$ radicals was greater during the second mopping event, consistent with the higher concentration of both monoterpenes and $O_3$ during this event. During the mopping events, 5 to 10 ppb of $O_3$ were sufficient to induce indoor SOA formation from ozonolysis (Fig. 2, E and F), notably less $O_3$ than previously reported to induce SOA either in a reaction chamber or under indoor-relevant conditions (*4*, *7*, *8*, *12*, *13*, *17*). Similar results were observed by Pagonis *et al.* (*27*) who found that a comparable level of $O_3$ (approximately 5 ppb) was enough to induce SOA formation from the ozonolysis of limonene emitted by peeling a navel orange inside a university art museum.

Gas-phase oxidation products were also observed immediately after the mopping period, and select products are shown in Figs. 2D and 3. Previous work, such as that of Leungsakul *et al.* (*4*), used a combination of modeling and chamber measurements to outline a semiexplicit mechanism of limonene and have identified limonaldehyde and limononic acid as major products of gas-phase ozonolysis. Similarly, Hammes *et al.* (*5*) used a high-resolution time-of-flight chemical ionization mass spectrometer with a filter inlet for gases and aerosols to determine that carboxylic acids dominate the gas-phase products from limonene ozonolysis. In the current work, Fig. 2D shows the real-time increase in $C_{10}H_{16}O_2$ (possibly limonaldehyde, from limonene oxidation; pinonaldehyde, from α-pinene oxidation; or a mixture of both; see table S2, labels 3A and 3B), $C_{10}H_{16}O_4$ (possibly a highly oxidized carboxylic acid; see table S2, label 1A), and $C_9H_{14}O_4$ [possibly limonic acid, ketolimononic acid, or another highly oxygenated organic molecule (HOM); see table S2, labels 5A to 5D] as detected by PTR-ToF-MS. Figure 3 (B to D) includes other highly oxidized, next-generation oxidation products (see ozonolysis mechanisms in figs. S3 and S4). A delay relative to the monoterpene trace in the increase and maxima of these oxidation products was observed, emphasizing their later emergence in the gas phase as secondary oxidation products resulting from monoterpene ozonolysis. On the other hand, while the decrease in the concentration of these oxidation products may be attributed to physical processes, such as air exchange, deposition, or gas-particle partitioning, some fraction of these gas-phase oxidation products may have undergone next-generation oxidation (Fig. 3, B to D) to yield HOMs that ultimately led to the observed indoor NPF events.

Indoor NPF was observed immediately after the formation of radicals and gas-phase oxidation products, as evidenced by the slight delay in the increase of particle number concentrations (Fig. 2, C to F). Here, we report the first direct measurements of the nucleation of sub–3-nm nanocluster aerosol (NCA) due to indoor monoterpene ozonolysis initiated using a terpene-based cleaner. Indoor NCA number concentrations increased rapidly to ~$10^5$ $cm^{-3}$ (Fig. 2F) and dominated the particle number size distributions during the first few minutes of the NPF event (Fig. 2E). The observed NCA number concentrations were generally similar to, or greater than, those reported during atmospheric NPF events in field and chamber studies (*38*).

The peak number concentration of the newly formed sub–3-nm particles was $0.91 \times 10^5$ and $5.76 \times 10^5$ $cm^{-3}$ during the first and second mopping episodes, high enough to grow rapidly into the nucleation and Aitken modes via condensation and coagulation, approaching modal diameters of approximately 30 nm in about 10 min after the start of the mopping period. This suggests particle growth rates of approximately 200 nm $hour^{-1}$, which is one to two orders of magnitude higher than those reported for typical atmospheric NPF events under different conditions but similar to selected observations reported in coastal areas (*39*). Sub–100-nm ultrafine particle number concentrations were sustained at around $10^5$ $cm^{-3}$ for the duration of the mopping events, which is similar to observations made during indoor combustion activities, such as cooking on a gas stove or lighting a candle (*2*), and outdoors in a traffic-impacted area (*40*). Peak number concentrations were higher by approximately an order of magnitude than previously observed in a similar indoor mopping experiment by Morawska *et al.* (*13*), possibly owing to a smaller room (140 $m^3$ versus 50 $m^3$ in this study) and measurement of particles down to 1.2 nm. The ozonolysis of skin oil has also been observed to initiate the formation of NCA in indoor environments (*41*). As one human volunteer was present during the cleaning episode, skin oil ozonolysis may have contributed to the measured NCA number concentrations. However, the contribution is expected to be small during cleaning-initiated monoterpene ozonolysis as the NCA number concentrations observed by Yang *et al.* (*41*) during skin oil ozonolysis in the presence of four human volunteers (~$1 \times 10^2$ to $5 \times 10^2$ $cm^{-3}$ for 35 to 40 ppb of $O_3$ at an AER of 3.2 $hour^{-1}$) are much lower than those measured here (~$10^5$ $cm^{-3}$).

The estimated aerosol mass fractions (AMFs) ranged from 0.31 to 0.88 for limonene and 0.17 to 0.24 for α-pinene (see the "Materials and Methods: Single-zone mass balance model for predicting SOA mass concentrations" section), which are within the range reported in chamber studies for terpene ozonolysis (*42*). Moreover, peak mass concentrations (for the 1.2 to 500 nm size range) were very close to the U.S. Environmental Protection Agency 24-hour guideline value for a particle pollution of 35 μg $m^{-3}$. The newly formed sub–100-nm particles that contribute little to particle mass, but dominate particle number, may be more health relevant because of their high efficiency of deposition in all regions of the respiratory system (fig. S8) and their propensity to penetrate to the deepest regions of the lung (see the "Human exposure implications of monoterpene ozonolysis during mopping" section).

It should be noted that in the current study, the AER was 4.5 $hour^{-1}$, approximately four times higher than in the study of Morawska *et al.* (*13*), showing that aerosol formation is rapid

enough that even a high AER in a small room is not sufficient to flush out secondary aerosols and their precursors or outweigh the rate of in situ particle nucleation and growth via condensation and coagulation. The current study room, while three times less in volume than the previously studied classroom, is similar to a typical office (*43*). The fourfold increase in AER was not able to compensate for the much faster rate of aerosol formation. This illustrates the tremendous aerosol formation capacity of high concentrations of monoterpenes and monoterpenoids in mechanically ventilated indoor environments during floor cleaning activities (Fig. 2, E and F).

Figure 3 illustrates other gas-phase oxidation products detected using the PTR-ToF-MS. Notably, these highly oxygenated products were present in the few parts per billion range (i.e., 0.1 to 1 ppb). Possible structures of these compounds are detailed in table S2. This list is not exhaustive; it only shows possible structures for oxygenated species that might have come from the oxidation of α-pinene, β-pinene, and limonene and that were detected by the PTR-ToF-MS.

### Background concentrations during nonmopping events

During nonmopping periods, background monoterpene concentrations were approximately 10 ppb, generally higher than that usually measured outdoors either in forested (*44*) or urban (*45*) areas. The exact identities of these monoterpenes are unknown, but previous studies have shown α- and β-pinene to be dominant monoterpenes in the surrounding forest (*35*) and thus may have influenced the indoor VOC composition via mechanical ventilation of outdoor air. It is also possible that there were indoor monoterpene sources within the building, such as wood waxes or polishes, or surfaces (wooden or otherwise) that off-gas into the recirculated air in the building, resulting in a background concentration.

$O_3$ concentrations continuously increased throughout the morning, starting from 5 ppb and increasing to 10 ppb around 13:00 (Fig. 2B). This range of $O_3$ concentrations is not unusual in enclosed indoor environments with natural ventilation (*7*, *17*, *33*). There were no known indoor $O_3$ sources inside the test room at the time of mopping, and thus, it is believed to predominantly have come from outdoor air via mechanical ventilation. The increasing upward diurnal trend is likely mirroring the diurnal trend in the outdoor $O_3$ concentration measured previously at this site [approximately 10 ppb at 09:00 and 45 ppb at 13:00 (*35*)]. The measured mixing ratios of $O_3$ and $NO_x$ were consistent with background measurements in other indoor environments (*33*).

Significant background concentrations of $HO_2$ and $RO_2$ radicals (~$10^8$ molecules $cm^{-3}$) were measured, similar to the ambient concentrations observed previously in the surrounding forest (*35*). They were most likely produced in situ, given that the background concentrations of 1 to 2 ppb of NO (fig. S2) result in peroxy radical chemical lifetimes of less than 5 s, and thus less likely introduced to the room via the mechanical ventilation system. Production of $HO_2$ and $RO_2$ may have come from background monoterpene concentrations oxidized by background $O_3$, subsequently producing both $RO_2$ and OH radicals. The latter can also oxidize VOCs as shown in Fig. 1 and thus produce more $RO_2$ and, subsequently, $HO_2$.

Nonzero background particle concentrations were most likely due to the transport of outdoor particles to the indoor environment via mechanical ventilation. The air handling unit (AHU) of the ventilation system included a minimum efficiency reporting value 8 filter, which generally has a low particle removal efficiency for sub–1000-nm particles (*46*). Thus, a significant fraction of outdoor particles entrained into the AHU were likely delivered to the test room during the experiments. To account for this entrainment of outdoor particles and other non-SOA–related sources, we introduced a source term $S_g$ into the SOA model (see Materials and Methods).

Although in situ SOA formation from background $O_3$ and monoterpene concentrations may be possible, there was a low background concentration of sub–10-nm particles. The number concentrations of 1.2- to 10-nm particles were approximately $10^2$ $cm^{-3}$ during background periods. In addition, because the initial concentration of background monoterpenes was low, the rate of ozonolysis was slower, and thus, the production of low-volatility oxygenated products was slower, favoring condensation onto preexisting particles rather than nucleation. Moreover, because the rate of the ozonolysis reaction was slower, losses of low-volatility compounds to indoor surfaces could become more important. This has been previously observed in chamber studies (*42*). While higher than that measured in other indoor environments (*7*, *17*, *33*), it is unlikely that the background concentrations of monoterpenes in this study affected the radical production and NPF observed during the mopping events.

## DISCUSSION

### SOA formation in low-$O_3$, high-VOC/AER small-volume indoor environments

As demonstrated in this study, the transport of outdoor $O_3$ to the indoor environment via a mechanical ventilation system results in background indoor $O_3$ concentrations, albeit being only a few parts per billion, that are still capable of driving indoor SOA formation. This is due, in part, to the high-VOC environment that is created during the active use of monoterpene-based cleaning products. As observed in Fig. 2, the sudden and pronounced increase in indoor monoterpene concentrations during mopping results in substantial NPF. Low-$O_3$, high-VOC indoor environments with high AERs, such as that established in the test room, can produce particle number concentrations similar to levels observed in traffic-affected outdoor areas, suggesting that custodial staff and people who clean frequently could be exposed to elevated particle concentrations even during brief cleaning periods indoors. This is further evidenced by the calculated respiratory tract deposited dose of SOA for humans during short mopping periods (discussed further in the "Human exposure implications of monoterpene ozonolysis during mopping" section). Also, the rapid formation of the particles in a small-volume indoor space (~50 $m^3$), albeit an AER 4.5 times higher than usual residential dwellings, may be indicative of the aerosol formation potential of individual offices, small apartments, or home microenvironments, such as individual kitchens, bedrooms, or bathrooms.

While residential dwellings may have a lower outdoor AER leading to lower indoor $O_3$ levels, the lower AER may lead to increased concentrations of reactive emissions during mopping episodes. An increased concentration of reactive emissions could offset the decrease in $O_3$ in the rate of ozonolysis and subsequent production of radicals and low-volatility oxygenated products (e.g., HOMs). If the production of HOMs were to change, then so would particle nucleation and growth rates, which tend to scale with HOM concentrations (*47*, *48*). Following the initial nucleation burst, lower AERs may affect the temporal evolution in the resulting SOA number size distributions (Fig. 2E). Patel *et al.* (*49*) found lower AERs to increase the coagulation rate of sub–10-nm particles,

thereby reducing their number concentrations, while increasing those of particles larger than 10 nm. Thus, under these conditions, NCA number concentrations may decay more rapidly than that observed in Fig. 2F. Last, if other indoor aerosol sources are present, then preexisting particle surface area concentrations will tend to increase as the AER is reduced. This will increase the condensation and coagulation sink of the preexisting particle population, which can enhance scavenging of low-volatility species and NCA, respectively, during the initial steps of the NPF event (*50*). Additional monoterpene ozonolysis experiments under varying building ventilation conditions will be needed to fully elucidate the role of the AER on indoor radical and SOA production.

## Comparison of measurements to model predictions

### *Model predictions of OH, $HO_2$, and $RO_2$ concentrations*

Figure 4 (A to C) shows the measured concentrations of OH, $HO_2$, and $RO_2$ radicals with concentrations predicted by the Master Chemical Mechanism (MCM version 3.3.1) for the ozonolysis of limonene and α- and β-pinene during the mopping events. Here, it is assumed that the composition of the monoterpene emissions is similar to that found in the cleaner (details described in Materials and Methods). While the OH measurements required signal averaging of approximately 1 hour to obtain values above the detection limit of the instrument, the observed values of $0.6 \times 10^6$ to $1.1 \times 10^6$ molecules $cm^{-3}$ agreed with the model predictions within the measurement uncertainty and precision (Fig. 3A). $HO_2$ radical concentrations were both predicted and measured to be similar during both mopping periods, confirming the small impact of photolytic processes on radical concentrations given the difference in sunlight exposure during the two events. While the measured $RO_2$ radical concentrations were in good agreement with the model predictions, the model underestimated the measured $HO_2$ concentrations by approximately a factor of 2, although the results were within the combined calibration uncertainty of the measurements [38%, 2σ (*35*)] and the estimated uncertainty of the model [30% (*35*, *51*)].

Differences in the timing of the measurements and the model are likely due to the time resolution of the instrument, as it alternates between measurements of $HO_2$ and $RO_2$ concentrations. The systematic difference between the measured and modeled $HO_2$ radical concentrations may suggest either a possible missing source of $HO_2$, additional recycling processes that are not accounted for in the MCM model, potential $RO_2$ interferences with the $HO_2$ measurements, or that the propagation rates converting $RO_2$ radicals to $HO_2$ (Fig. 1) may be underestimated in the model. The $RO_2$-to-$HO_2$ ratio can be used as a measure of the interconversion of peroxy radicals, and the measured and modeled $RO_2$-to-$HO_2$ ratios are shown in fig. S5. The model tends to overestimate the measured ratio by a factor of 2 to 3 during the mopping episodes, as well as during most of the background periods, suggesting that the model may be underestimating the rate of conversion of $RO_2$ to $HO_2$ in the ozonolysis mechanism both during the mopping and when constrained by the background concentrations. A recent theoretical study suggests that the peroxy radicals formed from the ozonolysis of limonene can undergo unimolecular reactions at rates fast

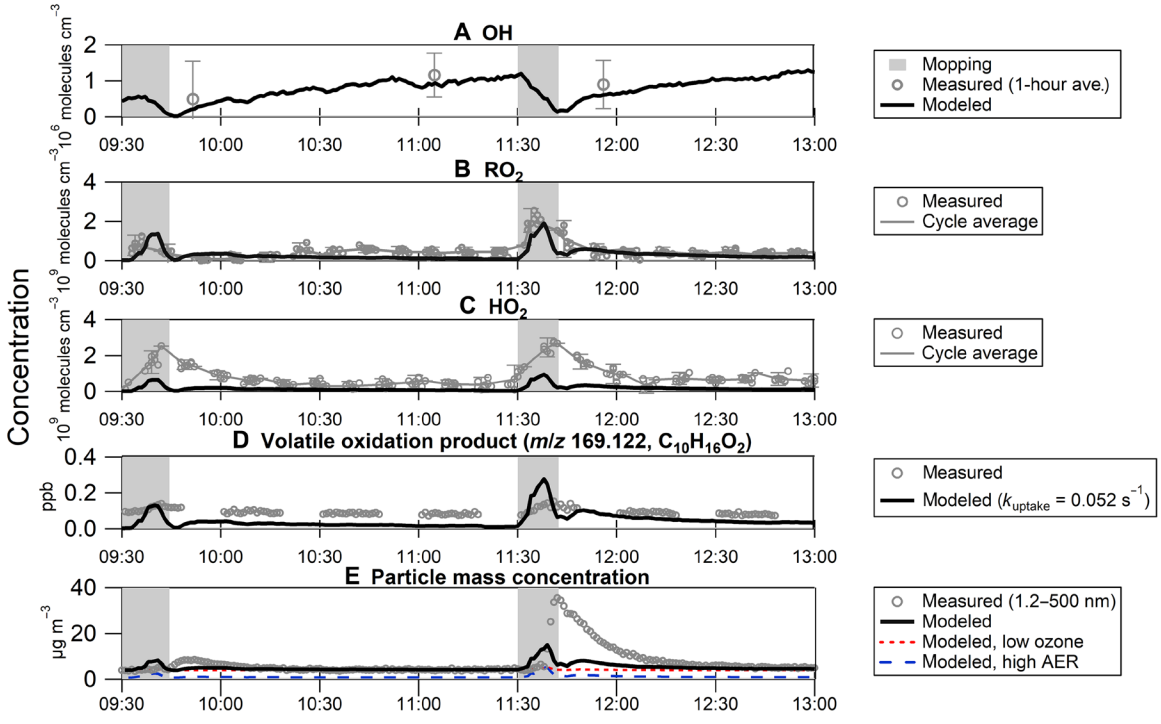


**Fig. 4. Measurements and model predictions.** (**A**) OH, (**B**) $RO_2$, (**C**) $HO_2$ radical, and (**D**) possible oxidation product (limonaldehyde, $C_{10}H_{16}O_2$) concentrations, and (**E**) size-integrated particle mass concentrations (1.2 to 500 nm) based on monoterpene, $O_3$, and $NO_x$ concentrations and $NO_2$ photolysis frequencies. Gray shading corresponds to active periods of mopping and wiping during the cleaning events. OH, $HO_2$, and $RO_2$ are compared to measured radical concentrations; OH values are close to the limit of detection and are shown here as 1-hour averages. Error bars shown are 1σ for OH and 2σ for $HO_2$ and $RO_2$. In (D), a pseudo first-order rate constant of $k = 0.052\ s^{-1}$ was taken to be representative of the loss to room walls and surfaces. In (E), a constant source rate of 18 μg $m^{-3}$ $hour^{-1}$ was considered. For the low-$O_3$ model, $O_3$ concentrations were divided 16-fold to reach a maximum concentration of 0.6 ppb. For the higher-AER model, the AER was increased to 24 $hour^{-1}$.

enough to compete with reactions with NO under typical indoor conditions (*52*). This is further supported by the experimental study of Pagonis *et al.* (*27*) in a university art museum, where measurements of indoor HOM production from limonene ozonolysis suggested that unimolecular isomerization was an important fate of $RO_2$ radicals under the low-NO conditions of this study.

In addition to leading to HOMs that can enhance SOA formation and growth, peroxy radical isomerization reactions could affect the propagation of $RO_2$ radicals to $HO_2$, reducing the $RO_2$-to-$HO_2$ ratio. It is not clear whether these $RO_2$ isomerization reactions are occurring in the mopping episodes reported here, as the mixing ratios of NO were higher than that observed by Pagonis *et al.* (*27*) (fig. S2). The rapid reaction of NO with $RO_2$ and $HO_2$ radicals produced from the ozonolysis mechanism likely explains why the mixing ratios of NO and $NO_2$ do not change as ozone decreases during the mopping episodes. While one might expect the concentration of NO to increase as ozone decreases given that the titration of NO by $O_3$ is rapid under these conditions, similar to that observed by Pagonis *et al.* (*27*), the decrease in the rate of NO + $O_3$ is likely offset by the increase in the reaction of NO with the elevated concentrations of $RO_2$ and $HO_2$ radicals, effectively buffering the NO (and $NO_2$) concentrations during the mopping episode. Additional measurements and modeling of these radicals under a range of NO concentrations are needed to fully test current mechanisms of indoor limonene ozonolysis.

### *Model predictions of gas-phase oxidation products from limonene ozonolysis*

Figure 4D compares the modeled and measured next-generation oxidation product (possibly limonaldehyde, $C_{10}H_{16}O_2$) that was detected in the gas phase with the PTR-ToF-MS during both mopping periods. This measured oxidation product can be taken as either limonaldehyde or pinonaldehyde or a combination of both. Incorporating a pseudo first-order heterogeneous loss onto room surfaces based on the uptake coefficient of pinonaldehyde (see Materials and Methods) improves the agreement of the model with the measurements (Fig. 4). Inclusion of autoxidation reactions for peroxy radicals that do not lead to limonaldehyde production may also improve the model agreement with the measurements (*27*, *52*). Another possible explanation for the difference between the measurements and the model is the unknown fragmentation patterns of many oxygenated products in the PTR-ToF-MS drift tube and sampling loss in the perfluoroalkoxy (PFA) tubing, the latter of which was not quantified. Here, only the mixing ratios of the parent ions of the gas-phase oxidation products are reported; thus, non-negligible fragmentation of limonaldehyde will result in measured mixing ratios that are less than the true values (sum of parent and fragment ions). Additional PTR-ToF-MS measurements and modeling studies are needed to resolve this discrepancy.

### *Predictions of indoor SOA mass concentrations*

Figure 4E shows the measured size-integrated (1.2 to 500 nm) SOA mass concentrations with that predicted by the single-zone mass balance model incorporating the ozonolysis of limonene and α- and β-pinene, the dominant terpenes detected in an analysis of the composition of the cleaner (see Materials and Methods and Eq. 2). While the simple model reproduces the production of SOA during the mopping episodes, it underestimates the observed peak SOA mass concentrations during the second episode by approximately a factor of 2.5, with the ozonolysis of limonene being the dominant contributor to the modeled mass concentrations. The reason for the discrepancy between the model and measurements is unclear but is likely due to the complex composition of the cleaning solution, as several potentially reactive compounds detected in the GC-MS analysis were not included in the simple model, such as α-terpineol, α-ionone, and myrcenol. Together, the ozonolysis of all the reactive compounds in the complex mixture could contribute significantly to the SOA mass concentrations. Ammonia ($NH_3$)–related particle growth, which is not accounted for in the model, may also contribute to the measured SOA mass concentrations (see the following section). Additional measurements and model simulations will be needed to fully characterize the individual contributions of the commercial cleaner to SOA formation.

While the current mass balance model can reasonably reproduce the measured SOA mass concentrations from monoterpene oxidation in indoor settings (Fig. 4E), a time delay of about 10 min for the first and about 5 min for the second event is noticeable. Previous experiments by Vartiainen *et al.* (*14*) have shown a time delay of 70 s from the time an orange was peeled in a room filled with $O_3$ before a concentration peak appeared for 3-, 7-, and 10-nm particles. Such a delay is likely due to a particle nucleation and growth phase period that is not reflected in the mass balance model. Notably, the formation of accumulation mode particles (100 to 500 nm), which contributed 65 to 83% to the measured SOA mass concentrations during the first mopping episode and 75 to 93% during the second, does not occur concurrently with the sudden increase in monoterpene concentrations and depletion of $O_3$. Rather, the indoor SOA mass in the accumulation mode is the result of particle growth beyond approximately 100 nm due to coagulation and condensation. As can be seen in Fig. 2E, the time evolution of the measured particle number size distributions into larger sizes takes several minutes, likely explaining the delay in timing of the peak SOA mass concentrations between the measurements and model output. SOA loss, largely driven by AER and deposition to indoor surfaces, was observed to be greater than the SOA source; however, some SOA mass is still being formed in situ because of condensation of low-volatility gases onto accumulation mode particles and coagulation of accumulation mode particles with sub–100-nm particles.

## Potential influence of human-associated emissions of ammonia and organic acids and outdoor sulfuric acid on indoor SOA production initiated by monoterpene ozonolysis

Ammonia ($NH_3$) has been shown to affect the condensational growth of monoterpene SOA via acid-base chemistry (*9*). Ammonium salts formed from the acid-base neutralization reaction between $NH_3$ and various organic acids can condense onto the newly formed SOA, promoting growth to larger sizes. As the limonene ozonolysis occurred in the presence of a human volunteer who performed the mopping sequence, human-associated emissions of $NH_3$ and organic acids may contribute to the observed particle growth. In an indoor environment, adults are estimated to emit 0.6 mg $hour^{-1}$ $person^{-1}$ of $NH_3$ (*53*); this would amount to 2.8 and 2.4 μg $m^{-3}$ (4.0 and 3.5 ppb) of $NH_3$ emitted during the first and second mopping events, respectively. Concentrations of various organic acids known to be associated with exhaled breath, skin secretions, skin oil ozonolysis, and the cleaning product itself exhibited notable increases during both mopping events (via PTR-ToF-MS; Fig. 3A and fig. S6). Thus, the abundance of $NH_3$ and organic acids in the test room may

have contributed to acid-based chemistry capable of enhancing indoor SOA mass.

Gas-phase sulfuric acid ($H_2SO_4$) plays an important role in the initial steps of atmospheric particle nucleation and growth (*54*). Outdoor $H_2SO_4$ may have been introduced into the indoor environment of the test room via the mechanical ventilation system, analogous to the transport of outdoor $O_3$ to indoor spaces. Outdoor $H_2SO_4$ has been measured previously at the field site with a diurnal average peak at $4 \times 10^6$ molecules $cm^{-3}$ during the daytime and about $2 \times 10^5$ to $3 \times 10^5$ molecules $cm^{-3}$ during nighttime (fig. S7). $H_2SO_4$ concentrations on the order of $10^5$ to $10^6$ molecules $cm^{-3}$ are within the range of those reported for field measurements of $H_2SO_4$-associated atmospheric NPF in forested environments (*55*). However, the extent to which $H_2SO_4$ concentrations are diminished because of loss processes during transport through the AHU remains unknown. $H_2SO_4$ and $NH_3$ have been shown to enhance multicomponent NPF through synergistic interactions with HOMs formed by the oxidation of isoprene and monoterpenes (*56*). Notably, particle nucleation rates tend to increase with $NH_3$ concentrations for mixtures containing $H_2SO_4$ and HOMs (*56*). Therefore, the delivery of outdoor $H_2SO_4$ to the $NH_3$-rich environment of the test room may have enhanced indoor NPF initiated by the ozonolysis of monoterpenes released from the cleaning product. Investigation into the contributions of human-associated emissions of $NH_3$ and organic acids and outdoor $H_2SO_4$ on indoor SOA production is needed to further understand the mechanisms that govern NPF in occupied, mechanically ventilated indoor environments.

### Human exposure implications of monoterpene ozonolysis during mopping

A multiphase inhalation exposure scenario during indoor mopping with a terpene-based cleaner in the presence of $O_3$ is illustrated in Figs. 5 and 6. First, one is exposed to the primary VOC emissions from the cleaning product. As illustrated in Fig. 5A, the time-resolved inhalation intake rate for gas-phase monoterpenes approaches 30 to 40 μg $min^{-1}$ shortly after initiation of the mopping sequence. For the duration of the active mopping period and subsequent concentration decay (90 min), this equates to 560 to 720 μg of inhaled gas-phase monoterpenes. Second, one is exposed to the indoor SOA formed in situ, starting from the freshly nucleated sub–3-nm NCA and continuing through its growth to larger sizes. Time-resolved and size-integrated inhalation intake rates for SOA (1.2 to 500 nm) were on the order of $10^9$ to $10^{10}$ inhaled particles $min^{-1}$ (number basis) and 0.1 to 0.7 μg $min^{-1}$ (mass basis) (Fig. 5B). Thus, one will inhale approximately $3.8 \times 10^{10}$ to $1.8 \times 10^{11}$ particles (3.0 to 7.5 μg) over the duration of a 90-min indoor mopping event, with much of the inhalation intake occurring during the first few minutes of active cleaning. The inhalation intake rates reported here are specific to the indoor environmental conditions under which the experiments were conducted (i.e., mass of cleaning product applied and test room AER). Thus, factors that act to increase or decrease gas- and aerosol-phase concentrations will also modulate the resulting exposure.

The fate of inhaled SOA in the human respiratory system is strongly size dependent. Inhalation exposure to indoor SOA can be better linked to cellular response in the lungs and respiratory health outcomes through calculation of size-resolved RTDDRs (*1*, *6*, *57*). Dose rates combine measured particle size distributions (Fig. 2E) with size-resolved deposition fractions (DFs) (fig. S8) to estimate the amount of inhaled SOA that deposits in each region of the respiratory system per unit time. Size-resolved number and mass dose rates for indoor SOA (1.2 to 500 nm) are illustrated in Fig. 6 (A and B) as $dRTDDR_N/dLogD_p$ ($min^{-1}$) and $dRTDDR_M/dLogD_p$ (μg $min^{-1}$), respectively; size-integrated dose rates are shown in Fig. 6 (C and D); and time-resolved cumulative deposited doses (time integration of dose rates) are shown in Fig. 5 (C and D).

The human respiratory system receives a significant dose of sub–30-nm SOA during indoor monoterpene ozonolysis events. Number dose rates are dominated by sub–30-nm particles and generally increase with decreasing particle size between 1.2 and 500 nm (Fig. 6A). The abundance of nanocluster and nucleation mode particles (Fig. 2F) during the indoor NPF events was associated with high dose rates in each region of the respiratory system. The magnitude of the total $dRTDDR_N/dLogD_p$ reached a maximum ($10^9$ to $10^{10}$ $min^{-1}$) in the sub–3-nm size fraction. The high number dose rates for sub–30-nm SOA are due to the prominent modes of the measured particle number size distributions (Fig. 2E) coinciding with submicrometer maxima in the DFs for the head airways (~1 nm), tracheobronchial region (~5 to 6 nm), and pulmonary region (~20 to 30 nm) (fig. S8). The efficient deposition of the newly formed sub–30-nm particles in the human respiratory system results in size-integrated number dose rates of $0.5 \times 10^9$ to $2.3 \times 10^9$ $min^{-1}$ (Fig. 6C); this equates to cumulative deposited doses on the order of $10^{11}$ particles over the duration of the two mopping events (Fig. 5C). The head airways receive the largest fraction of the total number dose rate and dose, followed by the tracheobronchial and pulmonary regions. Number dose rates were one to two orders of magnitude greater during the two mopping events as compared to background, unoccupied periods in the test room (Fig. 6C). During the latter, the primary source of indoor particles is the transport of outdoor particles indoors via mechanical ventilation.

In contrast to number dose rates, mass dose rates are dominated by accumulation mode particles (100 to 500 nm) (Fig. 6B) because of their meaningful contribution to particle mass size distributions during the SOA generation events. Size-integrated mass dose rates ranged from 0.024 to 0.054 μg $min^{-1}$, with much of the dose rate received in the pulmonary region (Fig. 6D). This is because DFs for the pulmonary region are greater than those for the head airways and tracheobronchial region for particles between 100 and 500 nm (fig. S8). The cumulative mass deposited dose reached approximately 3.0 and 7.5 μg after the first and second mopping events, respectively.

Indoor SOA production due to monoterpene ozonolysis during mopping results in dose rates greater than, or comparable to, what one would receive due to inhalation of traffic-associated aerosol (1.2 to 800 nm) (*58*) in an urban street canyon (Fig. 6, C and D). The size-integrated number dose rates during the first mopping event ($5.6 \times 10^8$ $min^{-1}$) was similar to that for an urban street canyon ($5.6 \times 10^8$ $min^{-1}$), whereas the second mopping event ($2.3 \times 10^9$ $min^{-1}$) was fourfold greater. In other words, exposure during 1.5 hours of mopping is equivalent to exposure to urban street canyon (traffic-influenced) air for 1.5 to 6 hours. Similarly, the size-integrated mass dose rate for the first (0.024 μg $min^{-1}$) mopping event was similar to that of the street canyon (0.025 μg $min^{-1}$), while that of the second mopping event (0.054 μg $min^{-1}$) was twice as high. The apportionment of the dose rates among the three regions of the respiratory system is similar between indoor-generated SOA and traffic-associated aerosol.

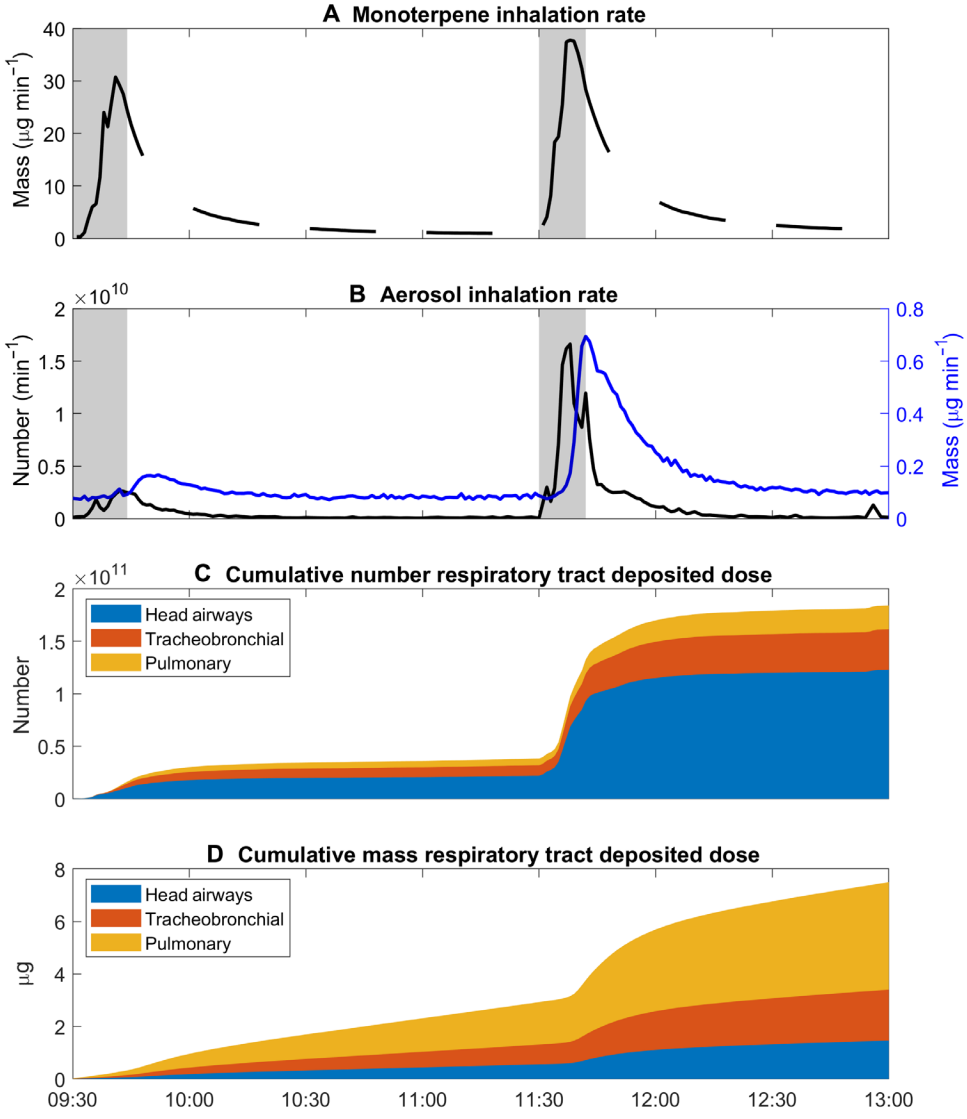


**Fig. 5. Time series of inhalation rates and cumulative respiratory tract deposited doses.** (**A**) Mass inhalation rate for monoterpenes, (**B**) size-integrated number (black) and mass (blue) inhalation rates for aerosols, (**C**) cumulative number respiratory tract deposited dose, and (**D**) cumulative mass respiratory tract deposited dose. The cumulative dose is taken as the time and size integration of $dRTDDR_{N/M}/dLogD_p$.

Sub–3-nm NCA contributed significantly to particle number size distributions (Fig. 2E) and corresponding number dose rates (Fig. 6A) during ozonolysis-initiated indoor NPF events. While recent observations have found an abundance of sub–3-nm particles in both indoor (*59*) and outdoor (*58*) environments, little is known regarding their toxicological profiles. Studies have found combustion-generated, organic sub–3-nm particles to cause significant cytotoxic response in mouse embryo fibroblasts (*60*), increase in cell mortality in human alveolar epithelial-like cells (*61*), and reduction in cell viability of endothelial cells (*62*). The high dose rate of sub–3-nm particles for the head airways (Fig. 6, A/C) is of concern, given the potential for nose-to-brain translocation (*63*). More broadly, the dominant role of sub–100-nm SOA toward number dose rates suggests a need for indoor exposure metrics based on particle number as such particles contribute little to particle mass (*64*).

Despite the uncertainty associated with indoor air toxicity and the toxicity of SOA produced from limonene ozonolysis, multiphase inhalation exposure during mopping with a terpene-based cleaner in the presence of $O_3$ is particularly of concern for janitors and building cleaners who spend considerable time each work period cleaning surfaces in indoor environments (*65*). As the cumulative deposited dose of SOA increases with exposure time (Fig. 5, C and D), repeated SOA generation events throughout a work period may pose an occupational health risk. Furthermore, workplace and residential exposures resulting in adverse health effects are likely to be influenced by increased chemical disinfection of indoor surfaces during the coronavirus disease 2019 pandemic (*66*). Selected terpene-based cleaning products containing glycolic acid, such as that evaluated in this study, have been shown to be effective in inactivating human coronaviruses, such as severe acute respiratory syndrome coronavirus 2

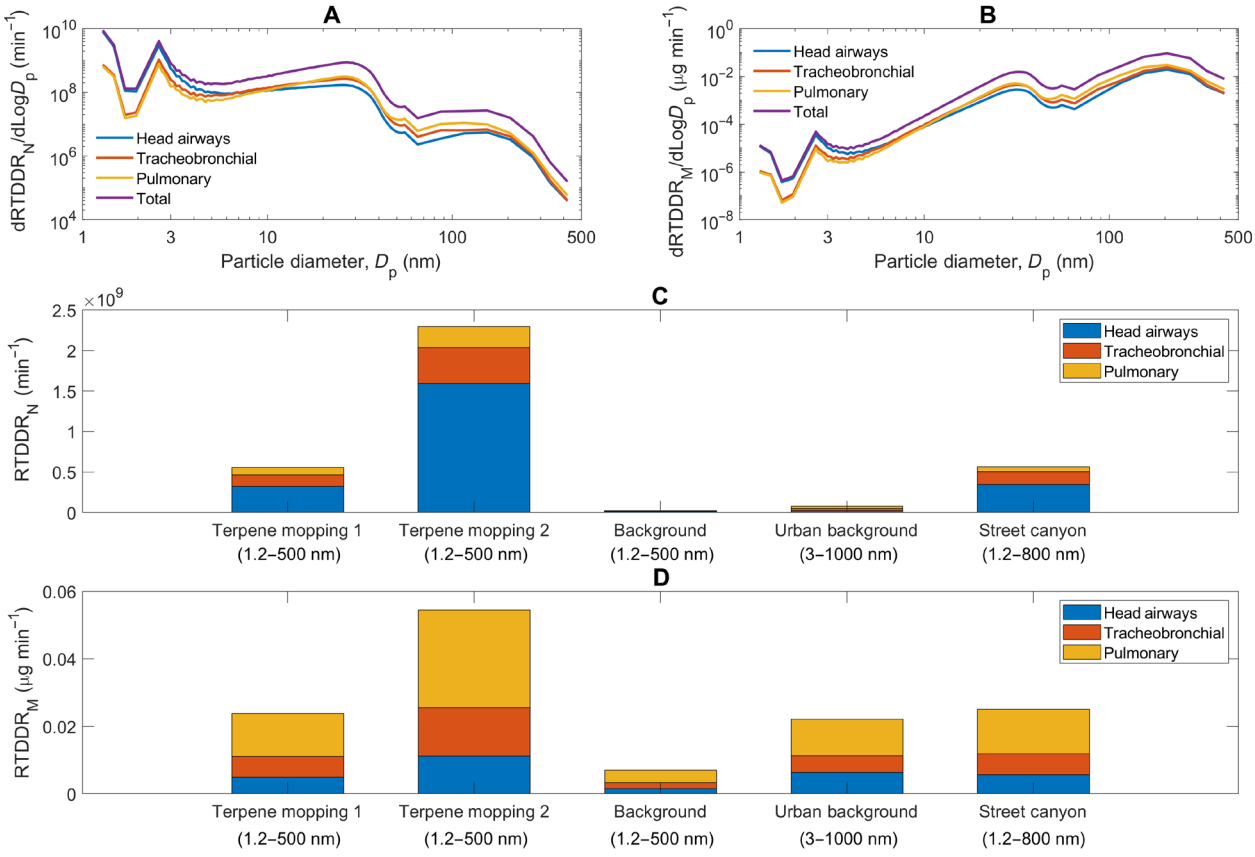


**Fig. 6. Regional and total RTDDRs.** (**A**) Size-resolved number RTDDRs ($dRTDDR_N/dLogD_p$) from 1.2 to 500 nm; (**B**) size-resolved mass dose rates ($dRTDDR_M/dLogD_p$) from 1.2 to 500 nm; and (**C**) size-integrated number and (**D**) mass dose rates for the two terpene mopping periods, background period in the test room before mopping, and outdoor urban and street canyon aerosol for comparison (*1*, *58*). The particle diameter from 1.2 to 2.5 nm is the activation diameter measured by the nCNC, the particle diameter from 2.5 to 300 nm is the electrical mobility diameter measured by the SMPS and NanoScan SMPS, and the particle diameter from 300 to 500 nm is the optical diameter measured by the optical particle sizer.

(SARS-CoV-2) (*66*). Recommendations to increase the outdoor AER in an effort to reduce airborne transmission of SARS-CoV-2 (*67*) could increase indoor $O_3$ concentrations at certain periods of the day (*26*) but would keep particle mass concentrations low throughout the day if $O_3$ does not build up indoors (Fig. 4E, blue dashed lines). Maintaining indoor background ozone levels below 1 ppb before cleaning events or emissions of terpenes would likely minimize particle mass concentrations produced during mopping periods (Fig. 4E, red dashed lines). Additional measurements and simulations using a more detailed indoor air chemical model are needed to confirm these results.

## MATERIALS AND METHODS

### Experimental design

The cleaning experiments were performed in a research building at the Indiana University Research and Teaching Preserve (IURTP). The IURTP field laboratory is located in a mixed deciduous forest consisting of sugar maple, sycamore, tulip poplar, ash, and hickory trees (*35*). It is located about 2.5 km northeast of the center of the Indiana University Bloomington campus and 1 km from the IN 45/46 bypass at the northern perimeter.

The research building is composed of a teaching classroom and several laboratory rooms. A fully enclosed room was chosen as the test room. The size of the chosen room is about 50 $m^3$, with a floor area of 20.5 $m^2$ and one northeast-facing window that received direct sunlight between 09:00 and 10:30. The AER for the test room during the experiments was 4.5 $hour^{-1}$ as measured via $CO_2$ tracer gas injection and decay. This AER was higher than most residential dwelling units [typically around 0.37 to 1.6 $hour^{-1}$ in urban areas, depending on ventilation conditions (*43*)] but within the range of what has been observed in some residential areas and in small and medium commercial buildings in the United States (*43*). Thus, the AER would be typical of an office space. The outdoor air was introduced into the room by a mechanical ventilation system with a damper-modulated outdoor air intake along the roof. This allowed for the introduction of ambient $O_3$ to the room.

A popular commercial household cleaner was used for mopping, containing limonene, camphene, and α- and β-pinene. Other listed ingredients included C10 alcohol ethoxylates, glycolic acid, pine oil, an unknown proprietary fragrance mixture, and hexyl cinnamal.

For the indoor cleaning episodes, a volunteer came in and mixed the cleaning solution inside the room. The recommended ratio of cleaner to water stated in the product label ($^1/_4$ cup per gallon of water) was followed. The volunteer then mopped the floors and wiped the surfaces with a cloth wetted with the cleaning solution. The cleaning episode was done for about 12 to 14 min, after which

the volunteer left the room and left the door and window closed for about 1 hour and 45 min.

## Measurements

### *OH, $HO_2$, and $RO_2$ radical measurements by laser-induced fluorescence*

OH, $HO_2$, and $RO_2$ radical concentrations were measured using a laser-induced fluorescence–fluorescence assay by gas expansion (LIF-FAGE) instrument (*35*). Two separate detection cells were used to measure the radicals. OH radicals were detected in one cell ("OH"; fig. S1) by LIF after expansion of ambient air to low pressure (5 torr) through a 1-mm pinhole inlet. The laser system used in this study was located in a separate room and consisted of a Nd:YAG laser (Spectra Physics) that produced approximately 8 W of radiation at 532 nm at a repetition rate of 10 kHz and is used to pump a dye laser (Sirah Credo) resulting in 40 to 100 mW of radiation at 308 nm. After exiting the dye laser, a fraction of the radiation is focused onto the entrance of a 12-m optical fiber to transmit the radiation to the sampling cell in the test room. OH radicals are excited and detected using the $A^2\Sigma^+ \upsilon' = 0 \leftarrow X^2\Pi \upsilon'' = 0$ transition near 308 nm, and the net signal is measured by spectral modulation by tuning the wavelength on- and off-resonance in successive cycles. A reference cell where OH is produced by thermal dissociation of water vapor is used to ensure that the laser is tuned on and off the OH transition. The OH fluorescence is detected using a microchannel plate photomultiplier tube detector (PMT325, Photek), which is switched off during the laser pulse through the use of electronic gating, allowing the OH fluorescence to be temporally filtered from laser-scattered light (*35*). The system is calibrated through the production of a known concentration of OH from the photolysis of water vapor at 185 nm as described previously (*35*).

$HO_2$ and $RO_2$ were measured in a second low-pressure detection cell with a reactor attachment ("$RO_x$LIF"; fig. S1). This attachment allows for the measurement of total $HO_2$ and $RO_2$ by CO/NO modulation (*68*). Ambient air enters the reactor through a pinhole inlet at a pressure of approximately 40 torr. The addition of CO to the reactor converts OH to $HO_2$, allowing for measurements of total $HO_x$ ($HO_2$ + OH). Addition of NO with CO also converts $RO_2$ radicals to $HO_2$, allowing for measurements of total $RO_x$ ($RO_2 + HO_2 + OH$). The converted $HO_2$ radicals are then introduced into the low-pressure detection cell, where NO is introduced through an injector to convert the $HO_2$ radicals to OH and the resulting OH radicals detected by LIF as described above. The sensitivity of the system to measure $HO_2$ radicals was calibrated as before by producing a known concentration of $HO_2$ radicals from the photolysis of water vapor at 185 nm in air. The sensitivity of the system to measured $RO_2$ radicals was calibrated by the addition of methane to the calibration source, converting the OH radicals produced from water vapor photolysis into a known concentration of $RO_2$ radicals (*68*).

### *Particle number size distribution measurements*

A suite of aerosol instruments was used to measure indoor particle number size distributions from 1.2 to 10,000 nm. Particles from 1.2 to 3 nm (activation diameter) were measured with a nano Condensation Nucleus Counter system (nCNC; A11, Airmodus Ltd.), which consists of a diethylene glycol–based particle size magnifier (PSM; A10, Airmodus Ltd.) and a butanol-based Condensation Particle Counter (bCPC; A20, Airmodus Ltd.) (*69*). The PSM can grow particles as small as 1 to about 90 nm, using diethylene glycol as the condensing fluid. After that, the bCPC further grows the particles to optical sizes and counts the number of particles. The nCNC was operated under scanning mode, in which the saturator flow rate was changed continuously from 0.1 to 1.3 liters $min^{-1}$ and then backward during a 240-s scan. The nCNC was calibrated using tube furnace–generated $(NH_4)_2SO_4$ and NaCl clusters size-classified with a Half-Mini differential mobility analyzer (DMA) (SEADM S.L.). A Scanning Mobility Particle Sizer (SMPS; model 3938NL88, TSI Inc.) consisting of an electrostatic classifier (model 3082, TSI Inc.) with a Kr-85 bipolar charger (370 megabecquerels, model 3077A, TSI Inc.), a nano DMA (model 3085, TSI Inc.), and a water-based CPC (model 3788, TSI Inc.) was used to measure particles from 2 to 65 nm (electrical mobility diameter) during a 120-s scan. A portable SMPS (NanoScan SMPS, model 3910, TSI Inc.) and an optical particle sizer (OPS; model 3330, TSI Inc.) measured particles from 10 to 420 nm (electrical mobility diameter) and 300 to 10,000 nm (optical diameter), respectively, at a sampling interval of 60 s. A High-Resolution Electrical Low Pressure Impactor (HR-ELPI+, Dekati Ltd.) with sintered collection plates was used to measure particles from 6 to 10,000 nm (aerodynamic diameter) at a rate of 1 Hz; however, the data are not included in this paper. No sample inlets were used for the aerosol instruments.

The raw data from the nCNC were processed using the expectation-maximization algorithm following Cai *et al.* (*70*). Selected nCNC size distributions were removed because of poor data quality. The raw data from the SMPS were corrected for diffusional losses due to particle transport within the SMPS (*71*). Particle number size distributions from the nCNC and SMPS were interpolated between minutes to be consistent with the 60-s sampling interval of the NanoScan SMPS and OPS. NanoScan SMPS size bins around 100 nm were saturated for multiple scans during the NPF events. The missing data were interpolated using data of adjacent size bins and scans. Data from all four instruments were merged to obtain a full particle number size distribution covering a size range from 1.2 to 10,000 nm. Size distributions between 1.2 and 2.5 nm, 2.5 and 56 nm, 56 and 300 nm, and 300 and 10,000 nm were derived from the nCNC, SMPS, NanoScan SMPS, and OPS, respectively. Particle mass size distributions were estimated from the measured number size distributions assuming an effective density of limonene ozonolysis SOA [1.3 g $cm^{-3}$ (*72*)]. In this study, size-integrated SOA mass concentrations were evaluated from 1.2 to 500 nm. Larger particles (e.g., 500 to 2500 nm) were excluded as they were likely generated from non–terpene ozonolysis processes in the test room, such as floor dust resuspension and particle release from the human envelope of the volunteer (*6*). There are uncertainties in the estimated particle mass size distributions due to interpolation and assumptions about particle morphology. Real-time direct measurements of particle mass size distributions in the accumulation mode would increase the accuracy of the measured SOA mass concentrations during the NPF events (*73*).

### *VOC measurements by PTR-ToF-MS*

VOCs from *m/z* 20 to 450 were measured at a rate of 1 Hz by a PTR-ToF-MS (PTR-TOF 4000, Ionicon Analytik Ges.m.b.H.) with a mass resolution >4000 m/Δm using $H_3O^+$ as the primary reagent ion. The instrument was operated at an electric field strength to gas number density ratio of 119 Td and an inlet temperature of 80°C. The sample gas flow rate was 80 standard cubic centimeters per minute. The temperature and pressure of the drift tube were maintained at 60°C and 2.2 mbar, respectively. The instrument background was determined twice daily using a cylinder of VOC-free

air (Matheson Tri-Gas Inc.), and the instrument was calibrated twice daily using two VOC gas standard mixtures (Apel-Riemer Environmental Inc.) containing 19 different compounds commonly measured in indoor air, including limonene, acetaldehyde, 6-methyl-5-hepten-2-one, decamethylcyclopentasiloxane, and decanal. During the calibration, the gas standards were diluted with VOC-free air to 2 to 40 ppb with a flow controller. The mass-dependent ion transmission was estimated from the daily calibrations. The total monoterpene concentration reported here (sum of signals at *m/z* 137 and 81), which includes contributions from the various monoterpenes detected in the liquid cleaning solution (limonene, α-pinene, β-pinene, and camphene), was calculated from the calibration with the limonene gas standard. Proton transfer reaction rate coefficients of various monoterpenes (limonene, α-pinene, β-pinene, and myrcene) vary within a relatively narrow range, from $2.2 \times 10^{-9}$ to $2.6 \times 10^{-9}$ $cm^3$ $s^{-1}$ (*74*–*76*). Thus, calculation of the total monoterpene concentration using the limonene gas standard would result in uncertainties of approximately 10%. For VOCs not included in the gas standard mixtures, concentrations were calculated on the basis of the proton transfer reaction theory, assuming a default reaction rate coefficient of $2 \times 10^{-9}$ $cm^3$ $s^{-1}$. This assumption results in uncertainties of <50% considering a common rate coefficient range from $1.5 \times 10^{-9}$ to $4 \times 10^{-9}$ $cm^3$ $s^{-1}$. Fragmentation patterns for the selected volatile oxidation products (Fig. 3) analyzed in this study are not available in the literature; thus, only mixing ratios of their parent ions were reported. Surface losses to the PFA sampling line were not quantified; however, they are expected to be negligible given the short residence time (~2 s) from the sampling inlet to the detector.

#### *Additional measurements*

$O_3$ was measured using a photometric analyzer based on ultraviolet absorption of $O_3$ at 254 nm (model M400E, Teledyne Technologies Inc.). $NO_x$ (NO and $NO_2$) was measured using a chemiluminescence-based analyzer that uses the characteristic luminescence resulting from the reaction of NO and $O_3$ (model 42C, Thermo Electron Corp.). To measure $NO_2$, the analyzer first converts $NO_2$ to NO using an internally heated converter and then reports concentrations as total $NO_x$. Hence, $NO_2$ is deduced by subtracting NO from the total $NO_x$ reported. Measurements of $J_{NO2}$ were made by a colocated spectral radiometer and used to determine additional photolysis frequencies in the model (*51*).

#### *Sampling locations and sequence*

The PTR-ToF-MS was connected to a "common-outlet" type, programmable multiport flowpath selector (EUTA-2VLSC8MWE2, Valco Instruments Co. Inc.) to enable for automated multilocation sampling between the test room and its mechanical ventilation system. A vacuum pump that was also connected to the selected stream outlet provided a constant carrier flow of approximately 9 liters $min^{-1}$. A rough pump was connected to the common outlet of the selector to prevent stagnant air by continuously drawing air through all unselected sampling lines. PFA tubes (0.952 cm outer diameter) were used as the sampling lines. At the intake of each sampling line, a polytetrafluoroethylene filter (1-μm pore size) was installed to remove particles. Sampling locations included indoor air in the test room, outdoor air and recirculation air intakes of the mechanical ventilation system serving the test room, and supply air to the test room. The 30-min sampling sequence started at XX:00 and XX:30 of every hour and was repeated as follows: indoor air in test room (20 min), outdoor air (3 min), recirculation air (3 min), and supply air (4 min). The LIF-FAGE, aerosol instruments, and $O_3$ and $NO_x$ analyzers only sampled room air for the duration of the mopping events reported in this study. The sampling location of each instrument in the room is shown in fig. S1.

#### *Analysis of the liquid cleaning solution via GC-MS*

The terpene-based cleaning solution was analyzed after experiment using GC-MS. Before injection, 1 ml of the cleaning solution was extracted using 100 ml of dichloromethane (DCM) using a separatory funnel; the bottom layer was then reextracted with 20 ml of DCM twice. This separation procedure was done for two 1-ml portions of the cleaning solution ($n = 2$). Standards were prepared for α-pinene, β-pinene, limonene, and myrcene by serial dilutions (solvent, DCM; final concentration, ~85 ng $ml^{-1}$). The samples and standards were then analyzed via GC-MS (GC HP6890, MSD 5973, Agilent) on an HP-5MS capillary column (30 m by 250 μm by 0.25 μm) with helium as the carrier gas and a flow rate of 1.2 ml $min^{-1}$. The injection volume was 1 μl (splitless mode), and inlet temperature was set to 285°C. The initial oven temperature was set to 70°C for the first 3.5 min, and then it was ramped up at a rate of 30°C $min^{-1}$; afterward, equilibration time was 6 min. The transfer line temperature was set at 285°C; the temperatures of the MS quad and ion source were 150° and 230°C, respectively. A full scan mode was used to obtain the spectra along the *m/z* range of 20 to 300.

### Modeling

#### *Zero-dimensional box model*

$HO_2$, $RO_2$, and OH were modeled with MCM v.3.3.1 chemical mechanism (*77*) using the Framework for 0-D Atmospheric Modeling (*51*). The base model calculates from a photochemical perspective and neglects transport and heterogeneous processes. To mimic indoor losses due to air exchange, a first-order rate constant for dilution was introduced. The model was constrained by 1-min averages of $O_3$, VOCs including monoterpenes, NO, $NO_2$, photolysis frequencies (scaled to the $J_{NO2}$ measurements), temperature, and relative humidity. Monoterpenes (i.e., α-pinene, β-pinene, and limonene) were appropriately scaled relative to their abundance measured in the cleaning solution using the GC-MS analysis (table S1). The ozonolysis of camphene was not included in the mechanism given that the ozonolysis rate constant is substantially lower than that for limonene, α-pinene, and β-pinene (table S1) (*78*).

The uptake of secondary products was investigated using limonaldehyde as a representative compound (Fig. 4D). The pseudo first-order rate constant, $k$, for the loss due to reactive uptake of limonaldehyde onto room surfaces can be estimated using the literature value of the uptake coefficient, γ, for pinonaldehyde, assuming that it is about the same as limonaldehyde ($\gamma = 1.3 \times 10^{-3}$) (*79*)

$$k = \frac{\gamma \langle c \rangle S}{4} \quad (1)$$

where $\langle c \rangle$ is the mean molecular speed of limonaldehyde, calculated to be 193 m $s^{-1}$, and $S$ is the surface area of the room, estimated to be approximately 21 $m^2$ per 50 $m^3$, not accounting for furniture and instruments in the room. Using these values, the calculated $k$ is 0.026 $s^{-1}$. Doubling this value ($k = 0.052$ $s^{-1}$) brings the modeled concentrations into better agreement with the measurements (Fig. 4D).

#### *Single-zone mass balance model for predicting SOA mass concentrations*

To model SOA mass concentrations produced in the room, a single-zone mass balance equation for a completely mixed flow reactor

adapted from Waring (*10*) was solved numerically (Eq. 2). In addition to chemical losses and production, the model incorporates room ventilation, particle deposition to surfaces, and the AMF

$$\frac{d[\mathrm{SOA}]}{dt} = (\mathrm{AMF}_{\mathrm{O_3+LIM}})\,k_{\mathrm{O_3+LIM}}[\mathrm{O_3}][\mathrm{LIM}]\Gamma_{\mathrm{terp\_LIM}} + (\mathrm{AMF}_{\mathrm{O_3+APIN}})\,k_{\mathrm{O_3+APIN}}[\mathrm{O_3}][\mathrm{APIN}]\Gamma_{\mathrm{terp\_APIN}} + (\mathrm{AMF}_{\mathrm{O_3+APIN}})\,k_{\mathrm{O_3+BPIN}}[\mathrm{O_3}][\mathrm{BPIN}]\Gamma_{\mathrm{terp\_BPIN}} - (\mathrm{AER} + \beta_{\mathrm{SOA}})[\mathrm{SOA}] + S_g \quad (2)$$

AMF was estimated using a previously observed empirical relationship of AMF versus the total organic aerosol mass concentration, $C_{OA}$ (*8*), which, in this case, was taken to be the sum of both background and newly formed aerosols. AMFs were estimated (derived via linear interpolation) from empirical relationships and parametrizations previously reported in the literature (*8*). For limonene, the derived AMFs were tuned by a factor of 2.5 to match the measurements and ranged from 0.31 to 0.88, which is within the range reported in previous terpene ozonolysis experiments in chambers (*8*). For α-pinene, the AMFs ranged from 0.17 to 0.24. For β-pinene, no AMFs were found in the literature; thus, α-pinene AMFs were used as a proxy. In Eq. 2, $k_{O3+LIM}$ is the rate constant for $O_3$ + limonene ($1.9 \times 10^{-2}$ $ppb^{-1}$ $hour^{-1}$) (*10*), $k_{O3+APIN}$ is the rate constant for $O_3$ + α-pinene ($7.56 \times 10^{-3}$ $ppb^{-1}$ $hour^{-1}$), and $k_{O3+BPIN}$ is the rate constant for $O_3$ + β-pinene ($1.32 \times 10^{-2}$ $ppb^{-1}$ $hour^{-1}$) (*78*). The terms [$O_3$], [LIM], [APIN], [BPIN], and [SOA] are the concentrations of $O_3$, limonene, α-pinene, β-pinene, and SOA mass, respectively. Proportions of limonene, α-pinene, and β-pinene were inferred from the GC-MS analysis and were taken to be 44, 10, and 16%, respectively (table S1). The contribution of camphene in the model was neglected given that the ozonolysis rate constant is approximately a factor of 100 to 200 times smaller than that for α-pinene and limonene (table S1) (*78*). $\Gamma_{terp}$ is a numerical conversion factor to convert from parts per billion to micrograms per cubic meter. The measured AER of 4.5 $hour^{-1}$ was used, and the aerosol first-order deposition loss rate coefficient ($\beta_{SOA}$) was estimated to be 0.1 $hour^{-1}$ (*10*). However, the contribution of $\beta_{SOA}$ to SOA mass loss in the test room was assumed to be negligible given that AER >> $\beta_{SOA}$ for accumulation mode particles (100 to 500 nm) that dominated the measured SOA mass concentrations. $S_g$ is a generic source rate, taken to be 18 μg $m^{-3}$ $hour^{-1}$, and is interpreted to be due to the delivery of outdoor particles to the test room via the mechanical ventilation system. In the absence of this generic source rate, the model is unable to reproduce the observed background particle mass concentrations from the ozonolysis of the measured background concentration of monoterpenes.

### *Size-resolved particle RTDDR analysis*

Size-resolved particle RTDDRs or inhaled deposited dose rates were analyzed to evaluate human exposure to SOA during the monoterpene mopping events. These dose rates describe the number or mass of particles that deposit in each region of the human respiratory tract (head airways, tracheobronchial region, and pulmonary region) per unit time (*1*, *6*, *57*). Briefly, dose rates were taken as the product of the measured number size distributions, or the estimated mass size distributions, with the inhalation rate and the size-resolved particle DF for each region of the respiratory tract. The inhalation rate was assumed to be 1.25 $m^3$ $hour^{-1}$ for an adult engaged in light activity, such as mopping and cleaning (*80*). This corresponds to an aerosol loss rate due to breathing of 0.02 $hour^{-1}$, suggesting that breathing was a negligible loss pathway for particles in the test room. Size-resolved particle DFs for an adult were obtained using the age-specific symmetric single-path model from the open-source Multiple-Path Particle Dosimetry model (v3.04, Applied Research Associates Inc.). Size-resolved dose rates in number ($RTDDR_N$, per minute) and mass ($RTDDR_M$, micrograms per minute) are represented as log-normal size distributions $dRTDDR_{N/M}/dLogD_p$. The total number and mass of particles deposited to the respiratory tract during a mopping event were estimated by integrating the RTDDRs over time and for different particle size fractions.

## SUPPLEMENTARY MATERIALS

Supplementary material for this article is available at https://science.org/doi/10.1126/sciadv.abj9156

## REFERENCES AND NOTES


1. T. Wu, B. E. Boor, Urban aerosol size distributions: A global perspective. *Atmos. Chem. Phys.* **21**, 8883–8914 (2021).
2. L. Wallace, Indoor sources of ultrafine and accumulation mode particles: Size distributions, size-resolved concentrations, and source strengths. *Aerosol Sci. Technol.* **40**, 348–360 (2006).
3. R. K. Pathak, K. Salo, E. U. Emanuelsson, C. Cai, A. Lutz, Å. M. Hallquist, M. Hallquist, Influence of ozone and radical chemistry on limonene organic aerosol production and thermal characteristics. *Environ. Sci. Technol.* **46**, 11660–11669 (2012).
4. S. Leungsakul, M. Jaoui, R. M. Kamens, Kinetic mechanism for predicting secondary organic aerosol formation from the reaction of d-limonene with ozone. *Environ. Sci. Technol.* **39**, 9583–9594 (2005).
5. J. Hammes, A. Lutz, T. Mentel, C. Faxon, M. Hallquist, Carboxylic acids from limonene oxidation by ozone and hydroxyl radicals: Insights into mechanisms derived using a FIGAERO-CIMS. *Atmos. Chem. Phys.* **19**, 13037–13052 (2019).
6. T. Wu, M. Täubel, R. Holopainen, A. K. Viitanen, S. Vainiotalo, T. Tuomi, J. Keskinen, A. Hyvärinen, K. Hämeri, S. E. Saari, B. E. Boor, Infant and adult inhalation exposure to resuspended biological particulate matter. *Environ. Sci. Technol.* **52**, 237–247 (2018).
7. S. Rossignol, C. Rio, A. Ustache, S. Fable, J. Nicolle, A. Même, B. D'Anna, M. Nicolas, E. Leoz, L. Chiappini, The use of a housecleaning product in an indoor environment leading to oxygenated polar compounds and SOA formation: Gas and particulate phase chemical characterization. *Atmos. Environ.* **75**, 196–205 (2013).
8. S. Youssefi, M. S. Waring, Transient secondary organic aerosol formation from limonene ozonolysis in indoor environments: Impacts of air exchange rates and initial concentration ratios. *Environ. Sci. Technol.* **48**, 7899–7908 (2014).
9. X. Niu, S. S. H. Ho, K. F. Ho, Y. Huang, J. Cao, Z. Shen, J. Sun, X. Wang, Y. Wang, S. Lee, R. Huang, Indoor secondary organic aerosols formation from ozonolysis of monoterpene: An example of d-limonene with ammonia and potential impacts on pulmonary inflammations. *Sci. Total Environ.* **579**, 212–220 (2017).
10. M. S. Waring, Secondary organic aerosol formation by limonene ozonolysis: Parameterizing multi-generational chemistry in ozone- and residence time-limited indoor environments. *Atmos. Environ.* **144**, 79–86 (2016).
11. B. C. Singer, B. K. Coleman, H. Destaillats, A. T. Hodgson, M. M. Lunden, C. J. Weschler, W. W. Nazaroff, Indoor secondary pollutants from cleaning product and air freshener use in the presence of ozone. *Atmos. Environ.* **40**, 6696–6710 (2006).
12. S. Langer, J. Moldanová, K. Arrhenius, E. Ljungström, L. Ekberg, Ultrafine particles produced by ozone/limonene reactions in indoor air under low/closed ventilation conditions. *Atmos. Environ.* **42**, 4149–4159 (2008).
13. L. Morawska, C. He, G. Johnson, H. Guo, E. Uhde, G. Ayoko, Ultrafine particles in indoor air of a school: Possible role of secondary organic aerosols. *Environ. Sci. Technol.* **43**, 9103–9109 (2009).
14. E. Vartiainen, M. Kulmala, T. M. Ruuskanen, R. Taipale, J. Rinne, H. Vehkamäki, Formation and growth of indoor air aerosol particles as a result of d-limonene oxidation. *Atmos. Environ.* **40**, 7882–7892 (2006).
15. T. Wainman, J. Zhang, C. J. Weschler, P. J. Lioy, Ozone and limonene in indoor air: A source of submicron particle exposure. *Environ. Health Perspect.* **108**, 1139–1145 (2000).
16. C. J. Weschler, H. C. Shields, Indoor ozone/terpene reactions as a source of indoor particles. *Atmos. Environ.* **33**, 2301–2312 (1999).
17. C. Rosch, D. K. Wissenbach, U. Franck, M. Wendisch, U. Schlink, Degradation of indoor limonene by outdoor ozone: A cascade of secondary organic aerosols. *Environ. Pollut.* **226**, 463–472 (2017).
18. N. Carslaw, A mechanistic study of limonene oxidation products and pathways following cleaning activities. *Atmos. Environ.* **80**, 507–513 (2013).

19. M. S. Waring, J. R. Wells, Volatile organic compound conversion by ozone, hydroxyl radicals, and nitrate radicals in residential indoor air: Magnitudes and impacts of oxidant sources. *Atmos. Environ.* **106**, 382–391 (2015).
20. R. Ciriminna, M. Lomeli-Rodriguez, P. Demma Cara, J. A. Lopez-Sanchez, M. Pagliaro, Limonene: A versatile chemical of the bioeconomy. *Chem. Commun. (Camb.)* **50**, 15288–15296 (2014).
21. S. K. Brown, M. R. Sim, M. J. Abramson, C. N. Gray, Concentrations of volatile organic compounds in indoor air—A review. *Indoor Air* **4**, 123–134 (1994).
22. U.S. Environmental Protection Agency, *Indoor Air Quality: Volatile Organic Compounds' Impact on Indoor Air Quality* (U.S. Environmental Protection Agency, 2020).
23. C. Wang, D. B. Collins, J. P. D. Abbatt, Indoor illumination of terpenes and bleach emissions leads to particle formation and growth. *Environ. Sci. Technol.* **53**, 11792–11800 (2019).
24. A. Wisthaler, C. J. Weschler, Reactions of ozone with human skin lipids: Sources of carbonyls, dicarbonyls, and hydroxycarbonyls in indoor air. *Proc. Natl. Acad. Sci. U.S.A.* **107**, 6568–6575 (2010).
25. H. Wang, G. C. Morrison, Ozone-initiated secondary emission rates of aldehydes from indoor surfaces in four homes. *Environ. Sci. Technol.* **40**, 5263–5268 (2006).
26. D. Lai, P. Karava, Q. Chen, Study of outdoor ozone penetration into buildings through ventilation and infiltration. *Build. Environ.* **93**, 112–118 (2015).
27. D. Pagonis, L. B. Algrim, D. J. Price, D. A. Day, A. V. Handschy, H. Stark, S. L. Miller, J. A. de Gouw, J. L. Jimenez, P. J. Ziemann, Autoxidation of limonene emitted in a university art museum. *Environ. Sci. Technol. Lett.* **6**, 520–524 (2019).
28. N. Carslaw, L. Fletcher, D. Heard, T. Ingham, H. Walker, Significant OH production under surface cleaning and air cleaning conditions: Impact on indoor air quality. *Indoor Air* **27**, 1091–1100 (2017).
29. M. Mendez, D. Amedro, N. Blond, D. A. Hauglustaine, P. Blondeau, C. Afif, C. Fittschen, C. Schoemaecker, Identification of the major $HO_x$ radical pathways in an indoor air environment. *Indoor Air* **27**, 434–442 (2017).
30. E. Gomez Alvarez, D. Amedro, C. Afif, S. Gligorovski, C. Schoemaecker, C. Fittschen, J. F. Doussin, H. Wortham, Unexpectedly high indoor hydroxyl radical concentrations associated with nitrous acid. *Proc. Natl. Acad. Sci.* **110**, 13294–13299 (2013).
31. S. D. Maleknia, T. L. Bell, M. A. Adams, PTR-MS analysis of reference and plant-emitted volatile organic compounds. *Int. J. Mass Spectrom.* **262**, 203–210 (2007).
32. J. Jiang, X. Ding, A. Tasoglou, H. Huber, A. D. Shah, N. Jung, B. E. Boor, Real-time measurements of botanical disinfectant emissions, transformations, and multiphase inhalation exposures in buildings. *Environ. Sci. Technol. Lett.* **8**, 558–566 (2021).
33. D. K. Farmer, M. E. Vance, J. P. D. Abbatt, A. Abeleira, M. R. Alves, C. Arata, E. Boedicker, S. Bourne, F. Cardoso-Saldaña, R. Corsi, P. F. DeCarlo, A. H. Goldstein, V. H. Grassian, L. Hildebrandt Ruiz, J. L. Jimenez, T. F. Kahan, E. F. Katz, J. M. Mattila, W. W. Nazaroff, A. Novoselac, R. E. O'Brien, V. W. Or, S. Patel, S. Sankhyan, P. S. Stevens, Y. Tian, M. Wade, C. Wang, S. Zhou, Y. Zhou, Overview of HOMEChem: House observations of microbial and environmental chemistry. *Environ Sci Process Impacts* **21**, 1280–1300 (2019).
34. X. Tang, P. K. Misztal, W. W. Nazaroff, A. H. Goldstein, Volatile organic compound emissions from humans indoors. *Environ. Sci. Technol.* **50**, 12686–12694 (2016).
35. M. M. Lew, P. S. Rickly, B. P. Bottorff, E. Reidy, S. Sklaveniti, T. Léonardis, N. Locoge, S. Dusanter, S. Kundu, E. Wood, P. S. Stevens, OH and $HO_2$ radical chemistry in a midlatitude forest: Measurements and model comparisons. *Atmos. Chem. Phys.* **20**, 9209–9230 (2020).
36. E. Ioannou, A. Koutsaviti, O. Tzakou, V. Roussis, The genus Pinus: A comparative study on the needle essential oil composition of 46 pine species. *Phytochem. Rev.* **13**, 741–768 (2014).
37. S. Kundu, B. L. Deming, M. M. Lew, B. P. Bottorff, P. Rickly, P. S. Stevens, S. Dusanter, S. Sklaveniti, T. Leonardis, N. Locoge, E. C. Wood, Peroxy radical measurements by ethane – nitric oxide chemical amplification and laser-induced fluorescence during the IRRONIC field campaign in a forest in Indiana. *Atmos. Chem. Phys.* **19**, 9563–9579 (2019).
38. J. Kontkanen, E. Järvinen, H. E. Manninen, K. Lehtipalo, J. Kangasluoma, S. Decesari, G. P. Gobbi, A. Laaksonen, T. Petäjä, M. Kulmala, High concentrations of sub-3nm clusters and frequent new particle formation observed in the Po Valley, Italy, during the PEGASOS 2012 campaign. *Atmos. Chem. Phys.* **16**, 1919–1935 (2016).
39. M. Kulmala, H. Vehkamäki, T. Petäjä, M. Dal Maso, A. Lauri, V. M. Kerminen, W. Birmili, P. H. McMurry, Formation and growth rates of ultrafine atmospheric particles: A review of observations. *J. Aerosol Sci.* **35**, 143–176 (2004).
40. Y. Zhu, W. C. Hinds, S. Kim, S. Shen, C. Sioutas, Study of ultrafine particles near a major highway with heavy-duty diesel traffic. *Atmos. Environ.* **36**, 4323–4335 (2002).
41. S. Yang, D. Licina, C. J. Weschler, N. Wang, N. Zannoni, M. Li, J. Vanhanen, S. Langer, P. Wargocki, J. Williams, G. Bekö, Ozone initiates human-derived emission of nanocluster aerosols. *Environ. Sci. Technol.* **55**, 14536–14545 (2021).
42. R. K. Pathak, C. O. Stanier, N. M. Donahue, S. N. Pandis, Ozonolysis of α-pinene at atmospherically relevant concentrations: Temperature dependence of aerosol mass fractions (yields). *J. Geophys. Res.* **112**, D03201 (2007).
43. R. Reichman, E. Shirazi, D. G. Colliver, K. G. Pennell, US residential building air exchange rates: New perspectives to improve decision making at vapor intrusion sites. *Environ Sci Process Impacts* **19**, 87–100 (2017).
44. N. C. Bouvier-Brown, A. H. Goldstein, J. B. Gilman, W. C. Kuster, J. A. de Gouw, In-situ ambient quantification of monoterpenes, sesquiterpenes, and related oxygenated compounds during BEARPEX 2007: Implications for gas- and particle-phase chemistry. *Atmos. Chem. Phys.* **9**, 5505–5518 (2009).
45. A. U. Raysoni, T. H. Stock, J. A. Sarnat, M. C. Chavez, S. E. Sarnat, T. Montoya, F. Holguin, W. W. Li, Evaluation of VOC concentrations in indoor and outdoor microenvironments at near-road schools. *Environ. Pollut.* **231**, 681–693 (2017).
46. B. Stephens, J. A. Siegel, Ultrafine particle removal by residential heating, ventilating, and air-conditioning filters. *Indoor Air* **23**, 488–497 (2013).
47. J. Kirkby, J. Duplissy, K. Sengupta, C. Frege, H. Gordon, C. Williamson, M. Heinritzi, M. Simon, C. Yan, J. Almeida, J. Tröstl, T. Nieminen, I. K. Ortega, R. Wagner, A. Adamov, A. Amorim, A. K. Bernhammer, F. Bianchi, M. Breitenlechner, S. Brilke, X. Chen, J. Craven, A. Dias, S. Ehrhart, R. C. Flagan, A. Franchin, C. Fuchs, R. Guida, J. Hakala, C. R. Hoyle, T. Jokinen, H. Junninen, J. Kangasluoma, J. Kim, M. Krapf, A. Kürten, A. Laaksonen, K. Lehtipalo, V. Makhmutov, S. Mathot, U. Molteni, A. Onnela, O. Peräkylä, F. Piel, T. Petäjä, A. P. Praplan, K. Pringle, A. Rap, N. A. D. Richards, I. Riipinen, M. P. Rissanen, L. Rondo, N. Sarnela, S. Schobesberger, C. E. Scott, J. H. Seinfeld, M. Sipilä, G. Steiner, Y. Stozhkov, F. Stratmann, A. Tomé, A. Virtanen, A. L. Vogel, A. C. Wagner, P. E. Wagner, E. Weingartner, D. Wimmer, P. M. Winkler, P. Ye, X. Zhang, A. Hansel, J. Dommen, N. M. Donahue, D. R. Worsnop, U. Baltensperger, M. Kulmala, K. S. Carslaw, J. Curtius, Ion-induced nucleation of pure biogenic particles. *Nature* **533**, 521–526 (2016).
48. J. Tröstl, W. K. Chuang, H. Gordon, M. Heinritzi, C. Yan, U. Molteni, L. Ahlm, C. Frege, F. Bianchi, R. Wagner, M. Simon, K. Lehtipalo, C. Williamson, J. S. Craven, J. Duplissy, A. Adamov, J. Almeida, A. K. Bernhammer, M. Breitenlechner, S. Brilke, A. Dias, S. Ehrhart, R. C. Flagan, A. Franchin, C. Fuchs, R. Guida, M. Gysel, A. Hansel, C. R. Hoyle, T. Jokinen, H. Junninen, J. Kangasluoma, H. Keskinen, J. Kim, M. Krapf, A. Kürten, A. Laaksonen, M. Lawler, M. Leiminger, S. Mathot, O. Möhler, T. Nieminen, A. Onnela, T. Petäjä, F. M. Piel, P. Miettinen, M. P. Rissanen, L. Rondo, N. Sarnela, S. Schobesberger, K. Sengupta, M. Sipilä, J. N. Smith, G. Steiner, A. Tomè, A. Virtanen, A. C. Wagner, E. Weingartner, D. Wimmer, P. M. Winkler, P. Ye, K. S. Carslaw, J. Curtius, J. Dommen, J. Kirkby, M. Kulmala, I. Riipinen, D. R. Worsnop, N. M. Donahue, U. Baltensperger, The role of low-volatility organic compounds in initial particle growth in the atmosphere. *Nature* **533**, 527–531 (2016).
49. S. Patel, D. Rim, S. Sankhyan, A. Novoselac, M. E. Vance, Aerosol dynamics modeling of sub-500 nm particles during the HOMEChem study. *Environ. Sci. Process. Impacts* **23**, 1706–1717 (2021).
50. R. Cai, D. Yang, Y. Fu, X. Wang, X. Li, Y. Ma, J. Hao, J. Zheng, J. Jiang, Aerosol surface area concentration: A governing factor in new particle formation in Beijing. *Atmos. Chem. Phys.* **17**, 12327–12340 (2017).
51. G. M. Wolfe, M. R. Marvin, S. J. Roberts, K. R. Travis, J. Liao, The Framework for 0-D Atmospheric Modeling (F0AM) v3.1. *Geosci. Model Dev.* **9**, 3309–3319 (2016).
52. J. Chen, K. H. Møller, P. O. Wennberg, H. G. Kjaergaard, Unimolecular reactions following indoor and outdoor limonene ozonolysis. *Chem. Eur. J.* **125**, 669–680 (2021).
53. M. Li, C. J. Weschler, G. Bekö, P. Wargocki, G. Lucic, J. Williams, Human ammonia emission rates under various indoor environmental conditions. *Environ. Sci. Technol.* **54**, 5419–5428 (2020).
54. J. Kirkby, J. Curtius, J. Almeida, E. Dunne, J. Duplissy, S. Ehrhart, A. Franchin, S. Gagné, L. Ickes, A. Kürten, A. Kupc, A. Metzger, F. Riccobono, L. Rondo, S. Schobesberger, G. Tsagkogeorgas, D. Wimmer, A. Amorim, F. Bianchi, M. Breitenlechner, A. David, J. Dommen, A. Downard, M. Ehn, R. C. Flagan, S. Haider, A. Hansel, D. Hauser, W. Jud, H. Junninen, F. Kreissl, A. Kvashin, A. Laaksonen, K. Lehtipalo, J. Lima, E. R. Lovejoy, V. Makhmutov, S. Mathot, J. Mikkilä, P. Minginette, S. Mogo, T. Nieminen, A. Onnela, P. Pereira, T. Petäjä, R. Schnitzhofer, J. H. Seinfeld, M. Sipilä, Y. Stozhkov, F. Stratmann, A. Tomé, J. Vanhanen, Y. Viisanen, A. Vrtala, P. E. Wagner, H. Walther, E. Weingartner, H. Wex, P. M. Winkler, K. S. Carslaw, D. R. Worsnop, U. Baltensperger, M. Kulmala, Role of sulphuric acid, ammonia and galactic cosmic rays in atmospheric aerosol nucleation. *Nature* **476**, 429–433 (2011).
55. S. L. Sihto, M. Kulmala, V. M. Kerminen, M. Dal Maso, T. Petäjä, I. Riipinen, H. Korhonen, F. Arnold, R. Janson, M. Boy, A. Laaksonen, K. E. J. Lehtinen, Atmospheric sulphuric acid and aerosol formation: Implications from atmospheric measurements for nucleation and early growth mechanisms. *Atmos. Chem. Phys.* **6**, 4079–4091 (2006).
56. K. Lehtipalo, C. Yan, L. Dada, F. Bianchi, M. Xiao, R. Wagner, D. Stolzenburg, L. R. Ahonen, A. Amorim, A. Baccarini, P. S. Bauer, B. Baumgartner, A. Bergen, A.-K. Bernhammer, M. Breitenlechner, S. Brilke, A. Buchholz, S. B. Mazon, D. Chen, X. Chen, A. Dias, J. Dommen, D. C. Draper, J. Duplissy, M. Ehn, H. Finkenzeller, L. Fischer, C. Frege, C. Fuchs, O. Garmash, H. Gordon, J. Hakala, X. He, L. Heikkinen, M. Heinritzi, J. C. Helm, V. Hofbauer, C. R. Hoyle, T. Jokinen, J. Kangasluoma, V.-M. Kerminen, C. Kim, J. Kirkby, J. Kontkanen, A. Kürten, M. J. Lawler, H. Mai, S. Mathot, R. L. Mauldin III, U. Molteni, L. Nichman, W. Nie,

T. Nieminen, A. Ojdanic, A. Onnela, M. Passananti, T. Petäjä, F. Piel, V. Pospisilova, L. L. J. Quéléver, M. P. Rissanen, C. Rose, N. Sarnela, S. Schallhart, S. Schuchmann, K. Sengupta, M. Simon, M. Sipilä, C. Tauber, A. Tomé, J. Tröstl, O. Väisänen, A. L. Vogel, R. Volkamer, A. C. Wagner, M. Wang, L. Weitz, D. Wimmer, P. Ye, A. Ylisirniö, Q. Zha, K. S. Carslaw, J. Curtius, N. M. Donahue, R. C. Flagan, A. Hansel, I. Riipinen, A. Virtanen, P. M. Winkler, U. Baltensperger, M. Kulmala, D. R. Worsnop, Multicomponent new particle formation from sulfuric acid, ammonia, and biogenic vapors. *Sci. Adv.* **4**, eaau5363 (2018).
57. T. Hussein, B. E. Boor, J. Löndahl, Regional inhaled deposited dose of indoor combustion-generated aerosols in jordanian urban homes. *Atmosphere* **11**, 1150 (2020).
58. T. Rönkkö, H. Kuuluvainen, P. Karjalainen, J. Keskinen, R. Hillamo, J. V. Niemi, L. Pirjola, H. J. Timonen, S. Saarikoski, E. Saukko, A. Järvinen, H. Silvennoinen, A. Rostedt, M. Olin, J. Yli-Ojanperä, P. Nousiainen, A. Kousa, M. Dal Maso, Traffic is a major source of atmospheric nanocluster aerosol. *Proc. Natl. Acad. Sci.* **114**, 7549–7554 (2017).
59. S. Patel, S. Sankhyan, E. K. Boedicker, P. F. DeCarlo, D. K. Farmer, A. H. Goldstein, E. F. Katz, W. W. Nazaroff, Y. Tian, J. Vanhanen, M. E. Vance, Indoor particulate matter during HOMEChem: Concentrations, size distributions, and exposures. *Environ. Sci. Technol.* **54**, 7107–7116 (2020).
60. L. A. Sgro, A. Simonelli, L. Pascarella, P. Minutolo, D. Guarnieri, N. Sannolo, P. Netti, A. D'Anna, Toxicological properties of nanoparticles of organic compounds (NOC) from flames and vehicle exhausts. *Environ. Sci. Technol.* **43**, 2608–2613 (2009).
61. L. Malorni, V. Guida, M. Sirignano, G. Genovese, C. Petrarca, P. Pedata, Exposure to sub-10 nm particles emitted from a biodiesel-fueled diesel engine: In vitro toxicity and inflammatory potential. *Toxicol. Lett.* **270**, 51–61 (2017).
62. P. Pedata, N. Bergamasco, A. D'Anna, P. Minutolo, L. Servillo, N. Sannolo, M. L. Balestrieri, Apoptotic and proinflammatory effect of combustion-generated organic nanoparticles in endothelial cells. *Toxicol. Lett.* **219**, 307–314 (2013).
63. G. J. Garcia, J. D. Schroeter, J. S. Kimbell, Olfactory deposition of inhaled nanoparticles in humans. *Inhal. Toxicol.* **27**, 394–403 (2015).
64. R. W. Baldauf, R. B. Devlin, P. Gehr, R. Giannelli, B. Hassett-Sipple, H. Jung, G. Martini, J. M. Donald, J. D. Sacks, K. Walker, Ultrafine particle metrics and research considerations: Review of the 2015 UFP workshop. *Int. J. Environ. Res. Public Health* **13**, 1054 (2016).
65. U.S. Department of Labor Bureau of Labor Statistics, Janitors and building cleaners, in *Occupational Outlook Handbook* (U.S. Bureau of Labor Statistics, 2021).
66. N. K. Rai, A. Ashok, B. R. Akondi, Consequences of chemical impact of disinfectants: Safe preventive measures against COVID-19. *Crit. Rev. Toxicol.* **50**, 513–520 (2020).
67. L. Morawska, J. W. Tang, W. Bahnfleth, P. M. Bluyssen, A. Boerstra, G. Buonanno, J. Cao, S. Dancer, A. Floto, F. Franchimon, C. Haworth, J. Hogeling, C. Isaxon, J. L. Jimenez, J. Kurnitski, Y. Li, M. Loomans, G. Marks, L. C. Marr, L. Mazzarella, A. K. Melikov, S. Miller, D. K. Milton, W. Nazaroff, P. V. Nielsen, C. Noakes, J. Peccia, X. Querol, C. Sekhar, O. Seppänen, S. I. Tanabe, R. Tellier, K. W. Tham, P. Wargocki, A. Wierzbicka, M. Yao, How can airborne transmission of COVID-19 indoors be minimised? *Environ. Int.* **142**, 105832 (2020).
68. H. Fuchs, F. Holland, A. Hofzumahaus, Measurement of tropospheric RO2 and HO2 radicals by a laser-induced fluorescence instrument. *Rev. Sci. Instrum.* **79**, 084104 (2008).
69. J. Vanhanen, J. Mikkilä, K. Lehtipalo, M. Sipilä, H. E. Manninen, E. Siivola, T. Petäjä, M. Kulmala, Particle size magnifier for nano-CN detection. *Aerosol Sci. Technol.* **45**, 533–542 (2011).
70. R. Cai, D. Yang, L. R. Ahonen, L. Shi, F. Korhonen, Y. Ma, J. Hao, T. Petäjä, J. Zheng, J. Kangasluoma, J. Jiang, Data inversion methods to determine sub-3 nm aerosol size distributions using the particle size magnifier. *Atmos. Meas. Tech.* **11**, 4477–4491 (2018).
71. J. E. Brockmann, Aerosol transport in sampling lines and inlets, in *Aerosol Measurement: Principles, Techniques, and Applications*, P. Kulkarni, P. A. Baron, K. Willeke, Eds. (Wiley, 2011), pp. 69–105.
72. H. Saathoff, K. H. Naumann, O. Möhler, Å. M. Jonsson, M. Hallquist, A. Kiendler-Scharr, T. F. Mentel, R. Tillmann, U. Schurath, Temperature dependence of yields of secondary organic aerosols from the ozonolysis of α-pinene and limonene. *Atmos. Chem. Phys.* **9**, 1551–1577 (2009).
73. V. Marple, B. Olson, F. Romay, G. Hudak, S. M. Geerts, D. Lundgren, Second generation micro-orifice uniform deposit impactor, 120 MOUDI-II: Design, evaluation, and application to long-term ambient sampling. *Aerosol Sci. Technol.* **48**, 427–433 (2014).
74. A. Tani, S. Hayward, C. N. Hewitt, Measurement of monoterpenes and related compounds by proton transfer reaction-mass spectrometry (PTR-MS). *Int. J. Mass Spectrom.* **223-224**, 561–578 (2003).
75. A. Tani, Fragmentation and reaction rate constants of terpenoids determined by proton transfer reaction-mass spectrometry. *Environ. Control. Biol.* **51**, 23–29 (2013).
76. J. Zhao, R. Zhang, Proton transfer reaction rate constants between hydronium ion (H3O+) and volatile organic compounds. *Atmos. Environ.* **38**, 2177–2185 (2004).
77. S. M. Saunders, M. E. Jenkin, R. G. Derwent, M. J. Pilling, Protocol for the development of the Master Chemical Mechanism, MCM v3 (Part A): Tropospheric degradation of non-aromatic volatile organic compounds. *Atmos. Chem. Phys.* **3**, 161–180 (2003).
78. R. Atkinson, D. Hasegawa, S. M. Aschmann, Rate constants for the gas-phase reactions of O3 with a series of monoterpenes and related compounds at 296 ± 2 K. *Int. J. Chem. Kinet.* **22**, 871–887 (1990).
79. J. Liggio, S.-M. Li, Reactive uptake of pinonaldehyde on acidic aerosols. *J. Geophys. Res.* **111**, (2006).
80. U.S. Environmental Protection Agency, "Exposure Factors Handbook: 2011 Edition (Final Report)" (EPA/600/R-09/052F, U.S. Environmental Protection Agency, 2011).
81. M. E. Jenkin, K. P. Wyche, C. J. Evans, T. Carr, P. S. Monks, M. R. Alfarra, M. H. Barley, G. B. McFiggans, J. C. Young, A. R. Rickard, Development and chamber evaluation of the MCM v3.2 degradation scheme for β-caryophyllene. *Atmos. Chem. Phys.* **12**, 5275–5308 (2012).
82. M. Glasius, M. Lahaniati, A. Calogirou, D. di Bella, N. R. Jensen, J. Hjorth, D. Kotzias, B. R. Larsen, Carboxylic acids in secondary aerosols from oxidation of cyclic monoterpenes by ozone. *Environ. Sci. Technol.* **34**, 1001–1010 (2000).
83. G. I. Gkatzelis, T. Hohaus, R. Tillmann, I. Gensch, M. Müller, P. Eichler, K. M. Xu, P. Schlag, S. H. Schmitt, Z. Yu, R. Wegener, M. Kaminski, R. Holzinger, A. Wisthaler, A. Kiendler-Scharr, Gas-to-particle partitioning of major biogenic oxidation products: A study on freshly formed and aged biogenic SOA. *Atmos. Chem. Phys.* **18**, 12969–12989 (2018).

**Acknowledgments:** We would like to thank P. Price (Indiana University) for helping with data analysis, Summer Undergraduate Research Fellow N. Khuu (Purdue University) for helping with the measurements, T. Wu (Purdue University) for calibrating the nCNC, M. Waring (Drexel University) and N. Donahue (Carnegie Mellon University) for insights on organic aerosol modeling, J. Flynn (University of Houston) for providing the radiometer to measure photolysis rates, R. (Lee) Mauldin III (University of Colorado Boulder) for providing the 2017 $H_2SO_4$ data (fig. S7), M. Chitwood of the IURTP for providing logistical support, and M. Venier and R. Hites of Indiana University for the supplementary analysis of the cleaning product via GC-MS.
**Funding:** This work was supported by the Alfred P. Sloan Foundation Chemistry of the Indoor Environments Program (G-2018-11061) (to P.S.S. and B.E.B.), the National Science Foundation (CBET-1847493) (to B.E.B.), and the Purdue Climate Change Research Center (to B.E.B.).
**Author contributions:** C.M.F.R. designed and scheduled the experimental procedure under the guidance of P.S.S. and B.E.B. J.J. and B.E.B. performed and analyzed the aerosol and PTR-ToF-MS measurements, with support from A.Ta. and H.H. C.M.F.R. and A.L. performed and analyzed the peroxy measurements. A.L., C.M.F.R., S.D., A.To., and P.S.S. developed the peroxy measurement technique. E.K.R., B.P.B., and V.K. performed the OH, $NO_x$, and $O_3$ measurements. B.P.B. performed the mopping procedures. C.M.F.R. did the modeling studies. J.J. did the RTDDR analysis. C.M.F.R., J.J., B.E.B., and P.S.S. wrote the manuscript with input from all coauthors. **Competing interests:** The authors declare that they have no competing interests. **Data and materials availability:** All data needed to evaluate the conclusions in the paper are present in the paper and/or the Supplementary Materials.

Submitted 10 June 2021
Accepted 10 January 2022
Published 25 February 2022
10.1126/sciadv.abj9156